https://doi.org/10.5194/acp-2020-1278
Preprint. Discussion started: 19 January 2021

Atmospheric Chemistry and Physics Discussions

Multi-dimensional satellite observations of aerosol properties and aerosol types over three major urban clusters in eastern China

Yuqin Liu[1], Tao Lin[1], Juan Hong[4], Yonghong Wang[3], Lamei Shi[2], Yiyi Huang[1,9], Xian Wu[1], Hao Zhou[1], Jiahua Zhang[2], Gerrit de Leeuw[5,6,7,8]

1 Key Lab of Urban Environment and Health, Institute of Urban Environment, Chinese Academy of Sciences, Xiamen 361021, China
2 Key Laboratory of Digital Earth Sciences, The Aerospace Information Research Institute, Chinese Academy of Sciences, Beijing 100094, China
3 Department of Physics, P.O. Box 64, 00014 University of Helsinki, Helsinki, Finland
4 Institute for Environmental and Climate Research, Jinan University, Guangzhou, Guangdong 511443, China
5 Royal Netherlands Meteorological Institute (KNMI), R&D Satellite Observations, 3730AE De Bilt, The Netherlands
6 Aerospace Information Research Institute, Chinese Academy of Sciences (AirCAS), No.20 Datun Road, Chaoyang District, Beijing 100101, China
7 Nanjing University of Information Science & Technology (NUIST), School of Atmospheric Physics, No.219, Ningliu Road, Nanjing, Jiangsu, China
8 University of Mining and Technology (CUMT), School of Environment Science and Spatial Informatics, Xuzhou, Jiangsu 221116, China
9 Coastal and Ocean Management Institute, Xiamen University, Xiamen 361102, China

Correspondence to: Tao Lin (tlin@iue.ac.cn), Jiahua Zhang(zhangjh@radi.ac.cn)

Abstract. Using nine years (2007-2015) of data from passive (MODIS/Aqua) and active (CALIOP/CALIPSO) satellite measurements over China, we investigate (1) the temporal and spatial variation of aerosol properties over the Beijing-Tianjin-Hebei (BTH) region, the Yangtze River Delta (YRD) and the Pearl River Delta (PRD) and (2) the vertical distribution of aerosol types and extinction coefficients for different aerosol optical depth (AOD) and meteorological conditions. The results show the different spatial patterns and seasonal variations of the AOD over the three regions. Annual time series reveal the occurrence of AOD maxima in 2011 over the YRD and in 2012 over the BTH and PRD; thereafter the AOD decreases steadily. Using the CALIOP vertical feature mask, the contributions of different aerosol types to the AOD were analysed: contributions of dust and polluted dust decrease from north to south, contributions of clean ocean, polluted continental, clean continental and smoke aerosol increase from south to north. In the vertical, the peak frequency of occurrence (FO) for each aerosol type depends on region and season and varies with AOD and meteorological conditions. In general, three distinct layers are observed with the peak FO at the surface (clean continental and clean marine aerosol), at ~1 km (polluted dust and polluted continental aerosol) and at ~3 km (smoke aerosol), whereas dust aerosol may occur all over the altitude range considered in this study (from the surface up to 8 km). In this study nighttime CALIOP profiles were used. The comparison with daytime profiles shows substantial differences in the FO profiles with altitude which suggest effects of boundary layer dynamics and aerosol transport on the vertical distribution of aerosol types.

1 Introduction

An aerosol is technically defined as a suspension of fine solid or liquid particles in a gas; common usage refers to the aerosol as the particulate component only (Seinfeld and Pandis, 1998). Aerosol particles are characterized by their diameter, chemical composition and shape (both are size-dependent), all of which vary with time and space (Unger et al., 2008; Shindell et al., 2009). Aerosol effects depend on particle size distribution, i.e. the number of particles of each size. Aerosol particles play an important role in the Earth's climate change and energy balance, directly by scattering and absorbing solar radiation and indirectly by modifying cloud properties and lifetime through their ability to serve as cloud condensation nuclei (Albrecht, 1989; Twomey, 1974; Andreae et al., 2004; Rosenfeld et al., 2008). Aerosol optical

https://doi.org/10.5194/acp-2020-1278
Preprint. Discussion started: 19 January 2021

Atmospheric Chemistry and Physics Discussions

depth (AOD), the column-integrated aerosol extinction coefficient, is often used as a proxy for the aerosol loading and air quality effects, and to assess the impact of aerosols on radiation, clouds and precipitation (Luo et al., 2014; Tian et al., 2017; Zhao et al., 2018; Liu et al., 2017; 2018). However, the aerosol indirect effects on climate are still poorly understood, much research is done on aerosol-cloud-precipitation interaction (Rosenfeld et al., 2014; Seinfeld et al., 2016; Zhou et al., 2016; Liu et al., 2017; Saponaro et al., 2017; Guo et al., 2018). The relative magnitudes and the sign of aerosol indirect effects are strongly influenced by aerosol types (IPCC, 2013; Rosenfeld et al., 2008; Yang et al., 2016; Massie et al., 2016), the aerosol vertical distribution (Heese et al., 2017; Zhao et al., 2018; Pan et al., 2019) and especially aerosol altitude relative to cloud layers (Costantino and Breon, 2013; Wang et al., 2015; Liu et al., 2017). Therefore, a systematic analysis of the temporal and spatial variations of aerosol concentrations, aerosol types and their vertical distribution is needed to better understand aerosol effects.

Many previous studies on the aerosol climatology and trends over China were conducted through ground-based remote sensing and satellite observations. Ground-based remote sensing includes the use of sun photometers in AERONET (Zhang and Li, 2019), SONET (Zhang and Li, 2015; Li et al., 2019; Zhang et al., 2020), CARSNET (Che et al., 2015), hand-held sun photometers in the CARE-China network (Xin et al., 2015) and solar radiation measurements (Xu et al., 2015). Satellite observations are made using, especially, MODIS (Moderate Resolution Imaging Spectroradiometer; Song et al., 2009; Tan et al., 2015; Ma et al., 2016; He et al., 2016) but also by multi-source satellite data (Lin et al., 2010; Guo et al., 2016; Dong et al., 2017; Zhang et al., 2017; Proestakis et al., 2018; de Leeuw et al., 2018; Sogacheva et al., 2018a,b; 2020). Other studies on the variation of aerosol types and vertical distribution of aerosols have been conducted through field campaigns (Schwarz et al., 2010; Kipling et al., 2013; Bauer et al., 2013; Samset et al., 2014; Wang et al., 2014; Kipling et al., 2016) and using ground-based lidars (He et al., 2008; Huang et al., 2008; Cao et al., 2013), although these have limited spatial coverage (e.g., Liu et al., 2012; Matthias et al., 2004). Since the launch of the Cloud-Aerosol Lidar with Orthogonal Polarization (CALIOP) aboard the Cloud-Aerosol Lidar and Infrared Pathfinder Satellite Observations (CALIPSO) in 2006 (Winker et al., 2009), the seasonal variations of aerosol types and the aerosol vertical distribution could be examined over large spatial scales, complementary to the local point measurements using ground-based lidars. Huang et al. (2013) examined the seasonal variations of aerosol type and extinction profiles using 5-years of CALIPSO lidar observations, including aerosol extinction coefficient, aerosol type, and maximum aerosol layer top height. Guo et al. (2016) investigated the three-dimensional (3D) structure of aerosols using the frequency of occurrence of aerosols derived from CALIOP observations over China. Tian et al. (2017) investigated the regional climatological aerosol vertical distributions and optical properties for eight representative regions over China. Zhao et al. (2018) examined the seasonal variations of aerosol column loading, vertical distribution, and aerosol types through combining datasets from multiple satellite sensors and ground-based observations during the period 2007-2016. Proestakis et al. (2018) used CALIOP data to create a 3-D climatology of dust aerosol over southeast Asia for 9 years (2007-2015), including the seasonality of dust transport pathways and dust layer heights, and dust-AOD trends. These previous studies mainly focused on the analysis of aerosol types and vertical distributions on global and regional scales. Only few studies focused on exploring the vertical distribution of different aerosol types under different aerosol conditions over China, especially over the urban clusters in eastern China. In addition, meteorology and large scale circulation have a strong effect on the vertical distribution

https://doi.org/10.5194/acp-2020-1278
Preprint. Discussion started: 19 January 2021

Atmospheric Chemistry and Physics Discussions

of aerosols, which usually further complicates aerosol indirect effects (He et al., 2008; Kipling et al., 2016; Guo et al., 2016b; Li et al., 2017; Kang et al., 2019; Hou et al., 2019; 2020). With the availability of long-term (2007-2015) measurements of aerosol properties, aerosol types and vertical profiles, together with ERA-Interim reanalysis data, the aerosol properties and vertical profiles over eastern China can be explored.

This study aims to investigate (1) the spatial and temporal variation of the AOD and the vertical distribution of aerosol types using multiple satellite datasets; (2) the vertical distribution of aerosol types and extinction coefficients for different atmospheric aerosol loading; (3) the effect of meteorological conditions on the vertical distribution of aerosol types. The study is conducted over three major urban areas in China, i.e. the BTH (Beijing, Tianjin and Hebei), the YRD (Yangtze River Delta) and the PRD (Pearl River delta), using MODIS and CALIOP data for the years 2007-2015. In this study, nighttime data are used. To put nighttime data in context, the day/night variation of the vertical distribution of aerosol types is discussed. This paper is organized as follows. Section 2 describes the study area, datasets used and data processing. Section 3 starts with a general description of the temporal and spatial variations of aerosol properties, followed by a description of the vertical distribution of aerosol types under different AOD conditions. In the latter we examine the impacts of different meteorological conditions on the vertical distribution of aerosol types. Also the difference between the vertical distributions of aerosol types during day- and night-time is discussed in Section 3. Major findings and conclusions are summarized in section 4.

2 Methods

2.1 Study area

Due to the rapid progress of urbanization and industrialization, eastern China has become one of the regions with the highest pollution in the world, and a hotspot for exploring direct and indirect effects of aerosols. The aerosol concentrations are very high with a variable and complex composition. Both direct aerosol emissions and secondary aerosol formation contribute to high concentrations of black carbon, other carbonaceous aerosols, sulfate, nitrate and dust aerosols, etc. High concentrations of aerosol particles over eastern China have strong implications on aerosol-cloud-climate interactions (Kourtidis et al., 2015), which are further complicated by the Asian monsoon system (Li et al., 2016). Eastern China is strongly influenced by the summer monsoon with precipitation belts moving from southern China in early April to northern China in July, and back to southern China in August. The monsoon influences aerosol transport and wet deposition (Liu et al., 2011; Luo et al., 2014), while in turn aerosol particles affect the distribution of precipitation and monsoon intensity (Li et al., 2016). Considering the occurrence of different aerosol types, their emission levels and meteorological and climate conditions, three regions were selected to examine the temporal and spatial variation of aerosol properties and their vertical distributions.

The Beijing-Tianjin-Hebei (BTH) (35.5°N-40.5°N, 113.5°E-120.5°E) area has a temperate monsoon climate, AOD is often high due to intensive human activities and can be augmented by the transport of desert dust in the spring. The Yangtze River Delta (YRD) (28°N-33°N, 117°E-122°E) is an area with a subtropical monsoon climate, which is regarded as a major source region of black carbon and sulfate (Wang et al., 2014; Andersson et al., 2015; Cheng et al., 2017). The Pearl River Delta (PRD) (21.5°N-24.5°N,

https://doi.org/10.5194/acp-2020-1278
Preprint. Discussion started: 19 January 2021

Atmospheric Chemistry and Physics Discussions

111.5°E-115.5°E) is an area with a tropical monsoon climate, which is influenced by both high anthropogenic aerosol emissions and a small fraction of marine aerosols (Streets et al., 2003, 2008; Lei et al., 2011; Xu et al., 2015; Heese et al., 2017).

2.2 Data sources

The MODIS sensor was launched by NASA (National Aeronautics and Space Administration, USA) aboard the Aqua satellite in 2002. It observes the Earth using 36 spectral bands from the UV to the thermal infrared and has a swath of 2330 km cross track, providing global coverage in 1-2 days. The Aqua equator crossing time is approximately 13:30 local time (ascending mode). For cloud-free pixels, three MODIS channels (0.47, 0.66 and 2.12 μm) are used to retrieve the AOD over land (Remer et al., 2005; Levy et al., 2013). Different algorithms are used to retrieve AOD from MODIS data, depending on the surface properties. Two dark target (DT) algorithms are used, one over vegetated/dark-soiled land, and another one over ocean, as described by Levy et al. (2013). Over bright surfaces, the deep blue (DB) algorithm is used (Hsu et al., 2004; 2013) which was enhanced to return AOD over all land types (Sayer et al., 2013; 2014). The AOD at 550 μm, obtained by interpolating between the AOD at 0.47 and 0.66 μm using the Ångström exponent, is one of the most widely used products in aerosol studies; it is publicly available at https://search.earthdata.nasa.gov/. Updates are regularly provided by the MODIS team at NASA and the most recent version is Collection 6.1 (C6.1) which was issued by the end of 2017. C6.1 is an improved version of C6. MODIS C6 was described in detail by Levy et al. (2013) and the AOD products over China were validated by, e.g., Tao et al. (2015), Shi et al. (2017) and de Leeuw et al. (2018). C6.1 merged DTDB AOD products over China were initially validated by Sogacheva et al. (2018a). Over China, the differences between the C6 and C6.1 AOD are small, except over certain areas like the Tibetan Plateau, Sichuan Province and the NW of China. Over the study area considered in the current study the C6 and C6.1 AOD are similar (see Fig. 6 in Sogacheva et al. 2018a). A comprehensive validation of the C6 and C6.1 DT AOD is presented in Che et al. (2019) and Bilal et al. (2019). More detailed information on the aerosol retrieval algorithms is available at http://modis-atmos.gsfc.nasa.gov. In this study, we use of the MODIS C6.1 level-2 merged product (C6.1 MYD04) (Levy et al., 2013), i.e. the merged DTDB AOD at 550 nm (from here on referred to as AOD) with a spatial resolution of 10×10 km^2 and better coverage than the individual DT or DB products. In this study, the daily MYD04 AOD data for the period January 2007-December 2015 were averaged to annual, seasonal and monthly values and used to analyze the temporal variations of the AOD on different time scales and the spatial distribution of the AOD in the three study regions.

CALIOP, launched onboard CALIPSO on April 28, 2006 is optimised for aerosol and cloud measurements (Winker et al., 2003). CALIOP is the first space-borne near-nadir dual-wavelength lidar (532 nm and 1064 nm). The 532 nm channel is polarisation sensitive. Its footprint is very narrow, with a laser pulse diameter of 70 m on the ground. The vertical resolution of the CALIOP product varies with altitude (h): 30 m for h =0 - 8.2 km, 60 m for h = 8.2 - 20.2 km, and 180 m for h = 20.2 - 30.1 km; the horizontal resolution is 333 m for altitudes from the surface up to 8.2 km, 1 km for altitudes ranging from 8.2 km to 20.2 km, and 1.667 km for altitudes from 20.2 km to 30.1 km. (Liu et al., 2009). In the current study the tropospheric column AOD is derived from the CALIOP 5 km aerosol layer products to examine patterns in the spatial distributions of aerosol types during different atmospheric pollution regimes in the three study areas (BTH, YRD and

https://doi.org/10.5194/acp-2020-1278
Preprint. Discussion started: 19 January 2021

Atmospheric Chemistry and Physics Discussions

PRD). The CALIOP level 2 vertical feature mask (VFM) 4.10 product provides the horizontal and vertical distributions of aerosol layers as well as the following aerosol sub-types: clean marine (sea salt), clean continental (clean background), polluted continental/smoke (urban/industrial pollution), elevated smoke (biomass burning aerosol), dust (desert), polluted dust (dust mixed with anthropogenic aerosol such as biomass burning smoke or urban pollution) and dusty marine (Kim et al., 2018). Daytime signals can be affected by background sunlight and reduce the SNR (signal to noise ratio), which may lead to underestimation of the frequency of occurrence (FO) of daytime aerosol types and a high bias in the daytime AOD, especially in the upper level (Huang et al., 2013). This is further illustrated with the comparison of vertical distributions of the FO of the aerosol types during day- and night-time overpasses. To avoid such problems, nighttime measurements at 532 nm were used in this study to investigate the vertical distribution of aerosol types and extinction coefficients. The vertical distribution of the frequencies of occurrence of CALIOP-derived aerosol types during nighttime are compared with those derived during daytime.

Meteorological parameters are used to examine the role of meteorological conditions on the vertical distribution of aerosol types. Global meteorological conditions with different spatial resolutions are available every six hours from the daily ERA Interim Reanalysis (http://apps.ecmwf.int/datasets/data/interim-full-daily/). Daily temperatures at the 1000 hPa and 700 hPa levels, relative humidity (RH) at the 950 hPa level and pressure vertical velocity (PVV) at the 750 hPa level on 0.125°×0.125° grids are used with the closest collocation with the CALIOP (nighttime) overpass time (18:00 UTC) over the study area.

https://doi.org/10.5194/acp-2020-1278
Preprint. Discussion started: 19 January 2021

Atmospheric Chemistry and Physics Discussions

2.3 Data processing

Aerosol properties are only retrieved for strictly cloud-free pixels, as determined using a cloud-detection scheme. However, because cloud detection schemes are not perfect, residual clouds may result in high AOD (Kaufman et al., 2005b). To avoid such problems, cases with MODIS AOD greater than 1.5 were discarded in the analysis. The CALIOP AOD is calculated using only data with quality control flags within the following limits: (1) 0 <= AOD_{532nm} <= 3.0; (2) -100 <= CAD_Score <= -20; (3) Ext_QC = 0, 1; and (4) 0 < AOD_{532nm}, unc/AOD_{532nm} <= 100%, where AOD_{532nm} is the aerosol optical depth at 532 nm wavelength, CAD_Score is the cloud-aerosol discrimination score, Ext_QC is the extinction quality control flag and $AOD_{532nm,unc}$ is the uncertainty of the AOD at a wavelength of 532nm. The CALIOP Feature_Classification_Flags were used to infer aerosol type occurrence at different altitudes in the troposphere. Prior to calculating the aerosol type variation, the aerosol layers with CAD scores between -100 and -20 were selected to ensure that only data of good quality were used. Meteorological conditions can affect the vertical aerosol variation such as transport of the aerosols from the lower atmosphere to elevated layers by heavy wind and deep convection (Yumimoto et al., 2009), long-range transport (Guo et al., 2016) or disconnected layers transported at different heights (Petäjä et al., 2016). Such conditions are explored using meteorological quantities which influence the aerosol properties; here, relative humidity (RH), lower tropospheric stability (LTS) and pressure vertical velocity (PVV) are considered.

3 Results and discussions

3.1 Yearly, seasonally and monthly variation of AOD

Time series of annually averaged AOD over the BTH, YRD and PRD for the years from 2007 to 2015 are presented in Figure 1(a). Over each of the three regions, the annually averaged AOD varies in a similar way, with the AOD over the PRD about 0.1 lower than over the BTH and the YRD. The AOD over the YRD was somewhat higher than over the BTH before 2010, whereas after 2011 the AOD over the BTH was highest. With interannual variations during the whole study period, the values in each region did not change much in the beginning of the study period. However, the AOD peaked in 2011 in the YRD and in 2012 in the PRD, with a broader plateau over the BTH during 2010-2012. After these years a declining trend started which continued until the end of the study period, as was also reported by Sogacheva et al. (2018a; b). This declining trend, which was largest over the PRD and smallest over the BTH, indicates that policy measures to control anthropogenic emissions of aerosols and precursor gases in China have been effective (Jin et al., 2016: van der A et al., 2017; Sogacheva et al., 2018b; He et al., 2018; Xie et al., 2019).

The seasonal variation of the AOD over the three regions is illustrated in Figure 1(b), which shows the AOD in each season averaged over the years 2007-2015, for each region. Here spring is defined as MAM, summer as JJA, autumn as SON and winter as DJF. The seasonal variation of the AOD is different in each region, and closer inspection shows that the main difference actually occurs in the

https://doi.org/10.5194/acp-2020-1278
Preprint. Discussion started: 19 January 2021

Atmospheric Chemistry and Physics Discussions

summer when the 9-year averaged seasonal AOD is lowest in the PRD (0.48) and highest in the BTH (0.81). In spring and autumn, the 9-year averaged AOD is similar in all three regions: around 0.69 in spring and about 0.51 in the autumn. In winter the AOD is similar to that in the autumn, with somewhat higher value in the BTH and a little lower in the other two regions. This seasonal variation is similar to that observed using ATSR and MODIS-Terra (C6 DTDB) AOD data averaged over 2000-2011 (de Leeuw et al, 2018). Different processes contribute to the differences in AOD among the 3 regions. During the summer, the direct emission of aerosols and precursor gases (contributing to secondary formation of aerosols) from straw burning contribute to the high AOD over the BTH. The high relative humidity during the summer monsoon in the BTH results in the growth of aerosol particles and shift of the particle size distribution to larger particles and thus an increase of the extinction and the AOD. Furthermore, the larger boundary layer heights (BLHs) in the summer allow for mixing over a deeper layer resulting in elevated AOD. BLHs are greatest over the BTH and smallest over the PRD (Guo et al., 2016b). In the spring, the high AOD over the YRD and BTH may be due to the contribution of long-range transported dust, while over the YRD also hygroscopic growth during elevated RH early in the monsoon season may contribute. The high AOD in the PRD in the spring may be related to long-range transport of pollutants from biomass burning in southeast Asia, which then mixes with moist air particles at the top of the boundary layer (Deng et al., 2008; Heese et al., 2017; Zhang et al., 2018). In the autumn the whole eastern region is dominated by westerly winds, which contributes to the diffusion of aerosols. Meanwhile, the impact of dust storms is relatively small in the autumn, which is also one of the reasons why the AOD is relatively low in this season. Conversely, during the winter, northerly winds prevail, bringing dry and clean air. In this situation the aerosol tends to be transported to the south and thus the aerosol concentrations over the BTH are reduced (Qi et al., 2013; Si et al., 2018). Hou et al. (2020) discuss four different synoptic situations giving rise to different transport schemes in east China resulting in either the accumulation or dissipation of aerosols in the BTH and YRD regions.

https://doi.org/10.5194/acp-2020-1278
Preprint. Discussion started: 19 January 2021

Atmospheric Chemistry and Physics Discussions

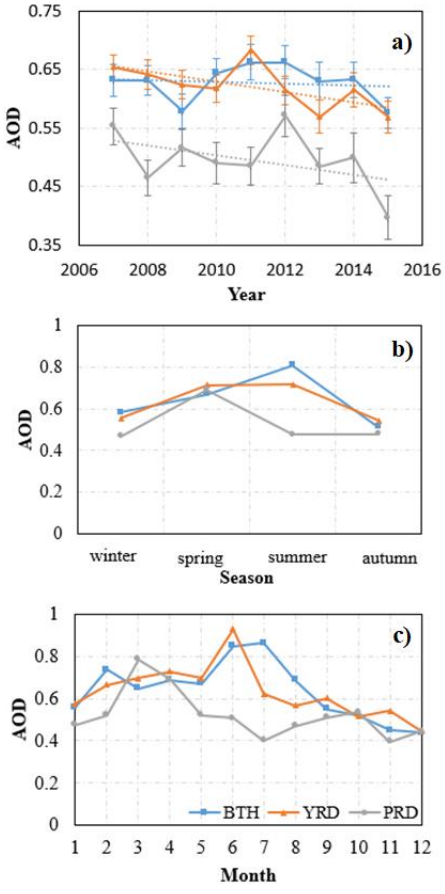

Figure 1. Annually (a), seasonally (b) and monthly (c) averaged AOD over the three study regions. The data for the three regions are color-coded.

The monthly AOD, averaged over the 9-years 2007-2015, over the three regions (Fig. 1(c)) shows that the largest differences between the regions occur from May to August. The summer AOD peak in the BTH occurs in July (AOD of 0.86), whereas in the YRD it clearly occurs in June (0.93) with a fast decline thereafter. In both regions, the AOD is higher in the period before the summer (0.6-0.7) and declines from September (0.6) to December (~ 0.4). In contrast, in the PRD the AOD peaks twice, in March (0.78) and in October (0.54), with much lower values in the summer and a clear minimum in July (0.4). The difference between the AOD variations in the three regions are due to processes discussed above for the seasonal variation, while in addition the effect of the East Asian summer monsoon moving from the south of China in April to the North in July and then back to the south affects the month-to-month variations (Luo et al., 2014). The monsoon brings heavy rains which effectively washout aerosols, resulting in the monthly AOD variations over the PRD with one peak before the pre-summer rain in March, the minimum during the summer rain period in July and the second AOD peak after the rainfall in October (Fig. 1(c)). With the seasonal progression of the monsoon to the north and weakening rainfall the monsoon arrives later in the year over the YRD and the BTH where the AOD

https://doi.org/10.5194/acp-2020-1278
Preprint. Discussion started: 19 January 2021

Atmospheric Chemistry and Physics Discussions

peaks occur in June and July, respectively.

3.2 Spatial variation of aerosol properties and aerosol types

3.2.1 Spatial variation of the MODIS AOD over major urban clusters

The spatial variation of the AOD over the three urban clusters, averaged over the seasons in the years from 2007 to 2015, is shown in Fig. 2. The spatial patterns over the three regions are similar in all seasons, but the values of the AOD vary from season to season. The AOD over the BTH is low over the mountains in Shanxi province in the Northwest and high in the Southeast over Hebei and Shandong. The mountains separate the North China Plan (NCP) in the east, with a very high degree of industrialization and a very high population density resulting in very high pollution, from the cleaner areas in the west. The mountains prevent the transport of pollution which accumulates along the ridge in meteorological conditions when the wind is from south-easterly directions, as observed all seasons. The heavy industries and power plants in the NCP are responsible for the high AOD. Meanwhile, the AOD in the summer may also be enhanced by emissions of aerosols and precursor gases from straw-burning (Kang et al., 2016a; Kumar et al., 2015; Si et al., 2018). Over the YRD, the AOD is lower in the Zhejiang and southern Anhui provinces as compared to other areas, during all seasons. The AOD is highest in the eastern part of the YRD, especially Shanghai and Jiangsu. There is a line with enhanced AOD going from Shanghai to the southwest of Zhejiang, i.e. over the Jin-Qu basin with high population density and much industrial activity. The AOD is lower over the mountains on both sides of the basin. The AOD spatial distribution over the PRD shows a ring-shaped pattern, with the highest values in the center and decreasing toward the outside of the ring. The highest AOD areas cover the busy industrial centers with much economic activity and a high number of vehicles, leading to elevated anthropogenic pollutants from coal, biomass burning and industrial emissions (Chen et al., 2014; Mai et al., 2018; Zhang et al., 2018).

https://doi.org/10.5194/acp-2020-1278
Preprint. Discussion started: 19 January 2021

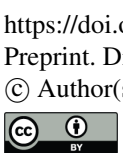

Atmospheric Chemistry and Physics Discussions

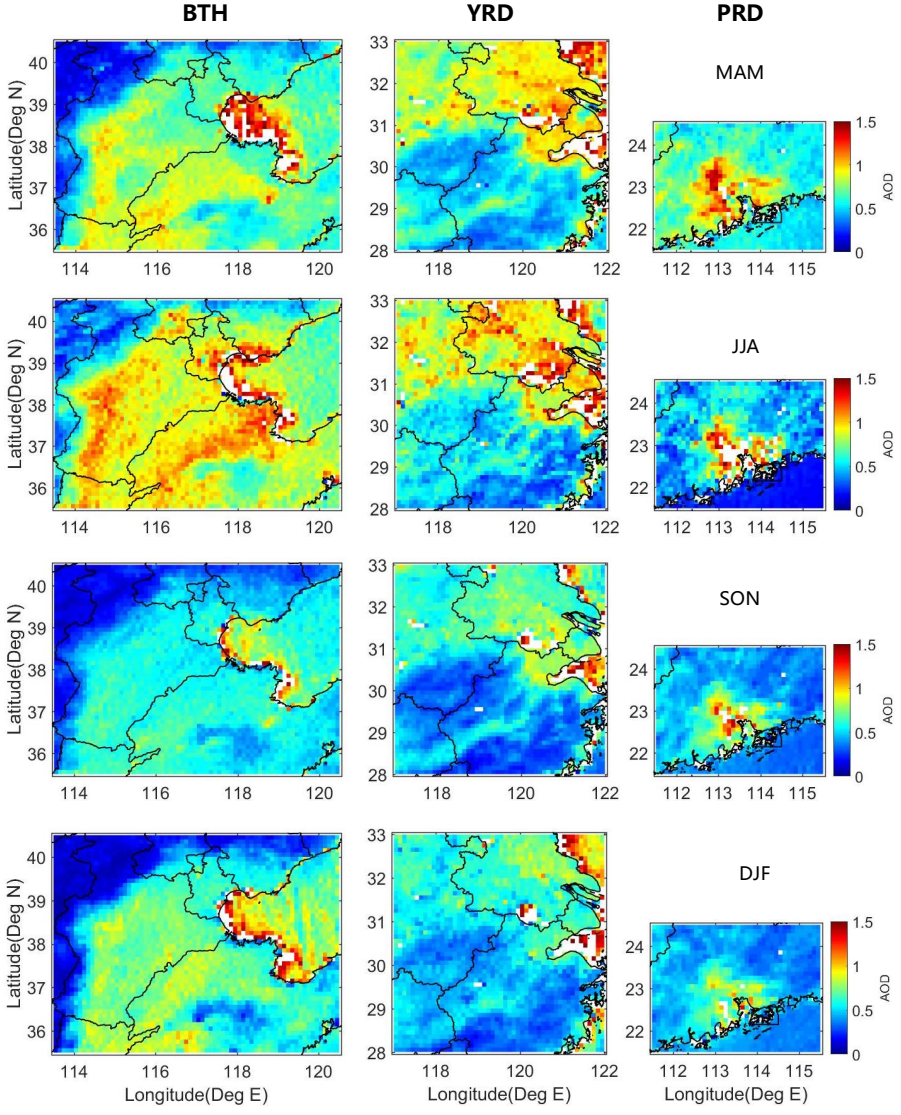

Figure 2 Spatial distributions of seasonally averaged AOD during the period from 2007 to 2015 over the BTH (left), YRD (middle), and PRD (right) for spring (MAM), summer (JJA), autumn (SON), and winter (DJF).

3.2.2 General distribution of aerosol types over major urban clusters

Aerosol types were obtained from the CALIOP VFM files (nighttime) over the three regions. The relative contribution of each aerosol type to the total aerosol burden in each of the three study areas was calculated by dividing the number of occurrences of each aerosol type in the whole vertical column by the total number of CALIOP aerosol observations. The results, averaged over the years 2007-2015, are presented in Fig. 3. Over the BTH, polluted dust aerosol is the most dominant aerosol type, with a contribution of 45% to the total aerosol population. Dust aerosol contributes 28%. These

https://doi.org/10.5194/acp-2020-1278
Preprint. Discussion started: 19 January 2021

Atmospheric Chemistry and Physics Discussions

numbers imply that the deserts in the northwest of China have a very large contribution to the total column-integrated aerosol over the BTH (Guo et al., 2016; de Leeuw et al., 2018). Polluted continental and smoke aerosol contribute 6% and 7%, respectively, to the total aerosol content. The contributions of clean marine and clean continental aerosol over the BTH are very small, with about 2% each.

Similar to the BTH, also over the YRD polluted dust (34%) and dust (23%) account for the largest fractions of the aerosol population. Polluted continental aerosol also contributes a substantial fraction (19%) to the total aerosol content. Smoke aerosol accounts for 19%. Clean marine and clean continental aerosol contribute only little over the YRD, with about 2% and 4%, respectively. The contribution of dusty marine aerosol has the lowest contribution over the YRD, with 2%.

The aerosol composition over the PRD is substantially different from that over the BTH and YRD, with a contribution of smoke aerosol of 30%. Polluted dust and polluted continental aerosol contribute 16% and 27%, respectively. In contrast to the other two regions, clean marine aerosol contributes substantially (14%) over the PRD and dust contributes only 3%. The contribution of clean continental aerosol is higher (6%) over the PRD than the other two regions. Although local anthropogenic pollution exerts a major influence on aerosols over the PRD, the northwest winter monsoon may transport continental aerosols (Heese et al., 2017), and the southeast summer monsoon may transport marine aerosols to this region (Wu et al., 2013; Heese et al., 2017).

These data show the large differences between the PRD and the other two regions. The frequencies of occurrence of clean marine, polluted continental, clean continental and smoke aerosol are lowest over the BTH and highest over the PRD. In contrast, polluted dust and dust contribute most to the aerosol over the BTH and very little over the PRD.

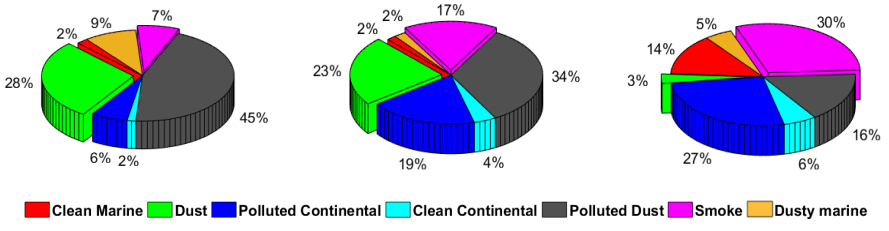

Figure 3. Contributions of different CALIOP aerosol types to the total aerosol content over the BTH (left), YRD (middle) and PRD (right), averaged over the time period 2007-2015.

3.3 Vertical distribution of aerosol types over major urban clusters

3.3.1 Vertical profiles of aerosol extinction coefficients during different AOD conditions

The vertical profiles of the aerosol extinction coefficients describe the variation of the attenuation of laser light (at 532 nm), due to scattering and absorption by aerosol particles, with altitude above the surface. Integration over the whole atmospheric column provides the AOD. Individual aerosol extinction profiles provide a measure for the vertical variation of aerosol concentrations, weighed by the optical properties of the aerosol particles, and modulated by the boundary layer. However, in this study, profiles obtained in certain conditions are averaged over the whole 9-year study period which

https://doi.org/10.5194/acp-2020-1278
Preprint. Discussion started: 19 January 2021

Atmospheric Chemistry and Physics Discussions

soothes the features and results in rather smooth profiles. This is illustrated in Fig. 4 which shows nighttime aerosol extinction coefficient profiles averaged over each of the three regions during moderately polluted, polluted and heavily polluted conditions (as determined by the AOD divided into three equally sized subsets). The extinction coefficient decreases monotonically from close to the surface up to about 2 km. The maximum occurring close to the surface is an artefact ascribed to the CALIOP retrieval algorithm which sets the aerosol base at 90 m above the surface to limit contamination due to surface effects on the lidar signal (Koffi et al., 2012). Above 2 km some structure is visible and at altitudes larger than 4 km some layering is observed, in particular in heavily polluted conditions over the PRD where distinct peaks are visible, which are likely due to single events with elevated aerosol layers. Aerosols are mainly situated in the atmosphere below 2 km with the maximum extinction coefficient near the surface (Tian et al., 2017). The extinction coefficient profiles are distinctly different, for both the different AOD conditions and over the three regions. As expected, the largest extinction coefficients occur in heavily polluted conditions and the lowest extinction coefficients in moderately polluted conditions, but the profile shapes are different in each of the three areas. Overall, the extinction coefficients are lowest over the PRD and highest over the YRD.

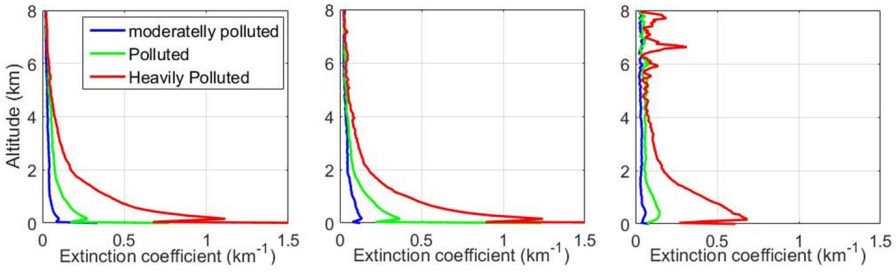

Figure 4 Aerosol extinction coefficient profiles over the BTH (left), YRD (middle) and PRD (right), grouped in different CALIOP AOD ranges as indicated by moderately polluted (top), polluted (middle) and heavily polluted (bottom), averaged over the years 2007-2015.

3.3.2 Vertical distributions of aerosol types in different seasons

Fig. 5 shows the vertical distribution of the frequency of occurrence (FO, in %) of the different aerosol types during nighttime over the three regions during the spring, summer, autumn and winter, averaged over the years 2007-2015. It is noted that these profiles show the frequency of occurrence of each aerosol type, normalized to the total sum of aerosol types over the whole profile, averaged per season over 9 years of observations. Hence the FO only indicates a relative number, i.e. ratio of the number of times a certainly aerosol type has been assigned by the VFM algorithm to the total number of times that any aerosol type was assigned. The FO profiles in Fig. 5 are averages over one of three regions during each of the four seasons. In these profiles, three different aerosol layers can be clearly distinguished with one or more dominating aerosol type and smaller contributions from other types. As indicated in Section 3.3.1, in the multi-year averages the concept of planetary boundary layer structure with mixed and residual layers with the free troposphere above (Stull, 1988) cannot be clearly distinguished.

https://doi.org/10.5194/acp-2020-1278
Preprint. Discussion started: 19 January 2021


Atmospheric Chemistry and Physics Discussions

Therefore we denote the three aerosol layers A, B and C. Layer A extends from the surface to about 2 km and does not have a distinct maximum. Layer B is interspersed with layer A and extends from the surface, where the FO is very small, to about 3 km, with a distinct maximum at about 1 km. Layer C extends from about 1.5 km to 4-5 km with a distinct FO peak around 3 km. In spring (MAM), layer C may extend to 6 km. As an example, this stratification is illustrated for the profiles over the PRD in the autumn (SON) where layer A contains clean marine and dusty marine aerosol, layer B contains polluted continental aerosol and layer C contains smoke and clean continental aerosol. Polluted dust aerosol occurs mainly in layer B with a small contribution in layer C. In addition, some aerosol types may occur over the whole column without a distinct layering (e.g. dust aerosol over BTH and YRD in the spring (MAM)) which is denoted as layer D.

The occurrence of aerosol in layer D likely indicates long-range transport of aerosol generated at or injected to higher altitudes and diffusing over the atmospheric boundary layer due to gravitation and other mixing processes. Such vertical mixing obviously affects all aerosol types and the occurrence of different types of aerosols in all three layers A-C which therefore contain different aerosol types with one or more dominating types. Upward mixing is however limited due to the occurrence of inversion layers which provide an effective lid on the layer below, while on the other hand convective mixing (e.g. in cloud systems) and the formation of disconnected layers may result in the occurrence of aerosol aloft. There are distinct differences in the vertical distributions between the three regions as well as between the seasons in each region.

The aerosol type over the BTH is dominated by polluted dust with a strong peak in layer B, which likely reflects the contribution of pollution, and substantially FO at higher altitudes (layer D), in particular in spring and summer when a peak is visible at an altitude of around 3 km (layer C). Layers C and D likely reflect the long-range transported dust component and the mixing with pollution due to upward transport. Dust is the second most important aerosol type over the BTH in all seasons except summer. In spring, dust occurs in all layers A-D and dominates at higher altitudes, i.e. from 1.8 km to as high as 8 km. In the winter, dust dominates above ~ 4 km. Smoke is important in the summer with a strong peak in layer C (above 2 km). Dusty marine aerosol is observed over the BTH in all seasons, mainly in layer A and extending from the surface up to 3-4 km, together with clean marine aerosol which has much smaller FOs and is negligible in spring. Polluted continental aerosol is observed in layer B, up to 2-3 km, and is the third most important aerosol type in the summer season.

Over the YRD, the dominating aerosol type varies with the seasons. The most abundant aerosol types in layer B are polluted dust, which dominates in the spring and winter, and polluted continental, which dominates in the summer and autumn. Polluted continental aerosol is confined to layer B, together with polluted dust which however extends higher up into layer C in the winter and spring to 7 and 8 km respectively (layer D), reflecting the influence of long-range transport. Dust is mainly observed in layers C and D and dominates in the winter and spring with the peak FO at about 5 km. This indicates that dust aerosol is often transported at high altitudes from north-west China across the mountains during westerly winds (Luo et al., 2014; Guo et al., 2016a; Proestakis et al., 2018). During the summer and autumn the dust FOs are not only much smaller but dust also occurs at lower altitudes. Smoke aerosol occurs below 4 km (layer C) where it dominates in the summer and autumn with a

https://doi.org/10.5194/acp-2020-1278
Preprint. Discussion started: 19 January 2021

maximum FO at about 3 km. Other aerosol types are observed with much smaller FOs over the YRD, with some clean marine aerosol in layer A and clean continental aerosol at somewhat higher elevations. Over the PRD, smoke (in the winter and spring) and polluted continental (in the summer and autumn) are the dominant aerosol types, while also clean marine aerosol is present in each season in layer A, from the surface up to about 2.5 km. Polluted continental aerosol is observed in layer B and smoke aerosol peaks at about 3 km (layer C), except in the spring when smoke aerosol dominates with relatively constant FOs in an extended layer between 2.5 and 4 km and decreasing toward the surface. Polluted dust occurs in layer B and, in the spring, the FO maximum occurs at about 4 km. Some clean continental aerosol is observed in layer C in all seasons. Dust is not prominent and mainly occurs with small FOs in layer C.

In general, the peak FO of polluted continental aerosols at an altitude of 1 km shows larger values over the PRD than that over the BTH and YRD. Moreover, polluted continental aerosol in the three target regions is always observed close to the ground (layer B) in all seasons (Liu et al., 2020). The peak FOs of polluted dust aerosols at lower altitude (at an altitude of about 1 km in layer B) in the three regions were highest in the winter. This may be explained by enhanced emissions due to the use of fossil fuel for domestic heating in the cold winter season and the mixing of the direct-emitted and secondary aerosol particles with long-range transported and locally generated dust particles. This effect may be enhanced during meteorological conditions conducive for the formation of haze (low windspeed, low inversion height) which often occur during winter time (Zhang et al., 2008; Tian et al., 2017). The FO of clean marine aerosols (layer A) is much higher over the PRD than in other regions in all four seasons, due to the vicinity of the ocean and the southeast summer monsoon which transports oceanic winds over the region.

https://doi.org/10.5194/acp-2020-1278
Preprint. Discussion started: 19 January 2021

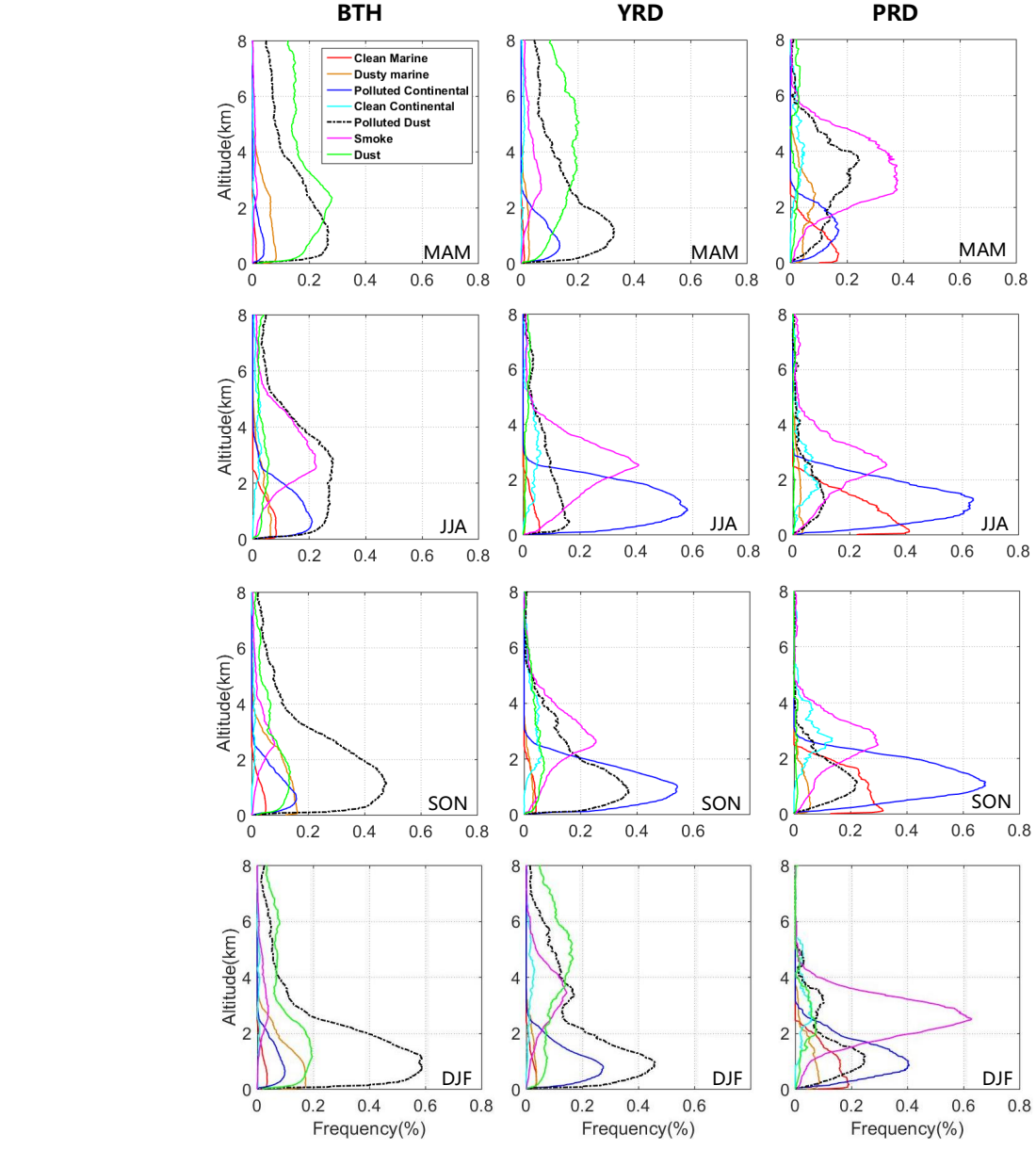

Figure 5. Vertical distribution of the FO of different CALIOP aerosol types by season over the BTH (top), YRD (middle) and PRD (bottom) averaged over the years 2007-2015.

3.3.3 Vertical profiles of aerosol types during different AOD conditions

Vertical profiles of night-time aerosol types grouped in different AOD ranges with equally sized subsets (as was done for extinction coefficient profiles in Fig. 4) are presented in Figure 6. Over the BTH, dominating aerosol types are polluted dust and dust, but the vertical distributions of the FO of

https://doi.org/10.5194/acp-2020-1278
Preprint. Discussion started: 19 January 2021


Atmospheric Chemistry and Physics Discussions

these types do not change much with increasing AOD. For polluted dust, in layer B, the depth of the layer increases somewhat with increasing AOD, whereas for dust the maximum FO increases with increasing AOD. However, the FOs of polluted continental aerosol, in layer A, and smoke aerosol, in layer C, increase substantially, whereas clean and dusty marine aerosol, both in layer A, are detected much less frequently in heavily polluted conditions than in the other two conditions.

Over the YRD, the dominating aerosol types in polluted and heavily polluted conditions are polluted continental and polluted dust, both in layer B with similar FO, but with polluted dust extending well above 2 km in layers C and D. The contribution of smoke aerosol in layer C increases somewhat with increasing pollution level. Dust aerosol also contributes substantially with little variation of the FO in the three conditions and also in the vertical. Clean marine aerosol, in layer A, has a substantial FO in moderately polluted conditions. The same applies to clean continental aerosol which however occurs mainly in layer C. In polluted and heavily polluted conditions the contributions of both these aerosol types are negligible.

Over the PRD, the aerosol in moderately polluted conditions is dominated by dusty marine aerosol, in layer A, with smaller contributions from smoke, polluted dust and clean continental aerosol (in order of decreasing FO), in layer C. Some polluted dust is also observed in layer B, with somewhat more polluted continental. With increasing pollution, the depth of layer A increases but the peak FO of dusty marine aerosol decreases to very small in heavily polluted conditions. The increase of pollution seems to be particularly caused by the strong increase of polluted continental aerosol in layer B and, to a lesser extent, smoke aerosol in layer C. Also the FO of polluted dust in layer B increases while it decreases higher up in layer C. Polluted continental, smoke and polluted dust strongly dominate the aerosol in heavily polluted conditions.

The data presented above show some clear differences over the three study regions. Over the BTH the influence of dust clearly dominates the degree of pollution, with both dust and polluted dust near the surface in layer B, extending to the top of the study area at 8 km. The effect of dust is smaller but clearly present in the YRD whereas in the PRD it is rather small. The effect of smoke in the free troposphere (layer C) is clear in all three regions, increasing with degree of pollution. Smoke effects are strongest over the PRD and smallest over the BTH. Similar considerations apply to polluted continental aerosol: increasing with increasing pollution with the largest effect over the PRD and the smallest effect over the BTH. The effect of marine aerosol (clean or dusty) is also present in all three study regions, but mainly in moderately polluted conditions and decreasing with distance to the ocean, i.e. large over the PRD and small over the BTH.

Generally, the peak FO of smoke aerosol over the three regions is largest in heavily polluted conditions. This can be attributed to the stronger efficiency of smoke aerosol particles for the absorption of sunlight, which increases the AOD (Small et al., 2011; Liu et al., 2017). What's more, the FO of smoke aerosol in low AOD conditions is distributed higher in the atmosphere over the three regions. A remarkable feature is that the vertical profiles of the dust aerosol FO show little variation in different AOD conditions over the three regions, except for an obviously decreasing height of the peak FO of dust aerosol over the YRD.

https://doi.org/10.5194/acp-2020-1278
Preprint. Discussion started: 19 January 2021

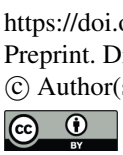

Atmospheric Chemistry and Physics Discussions

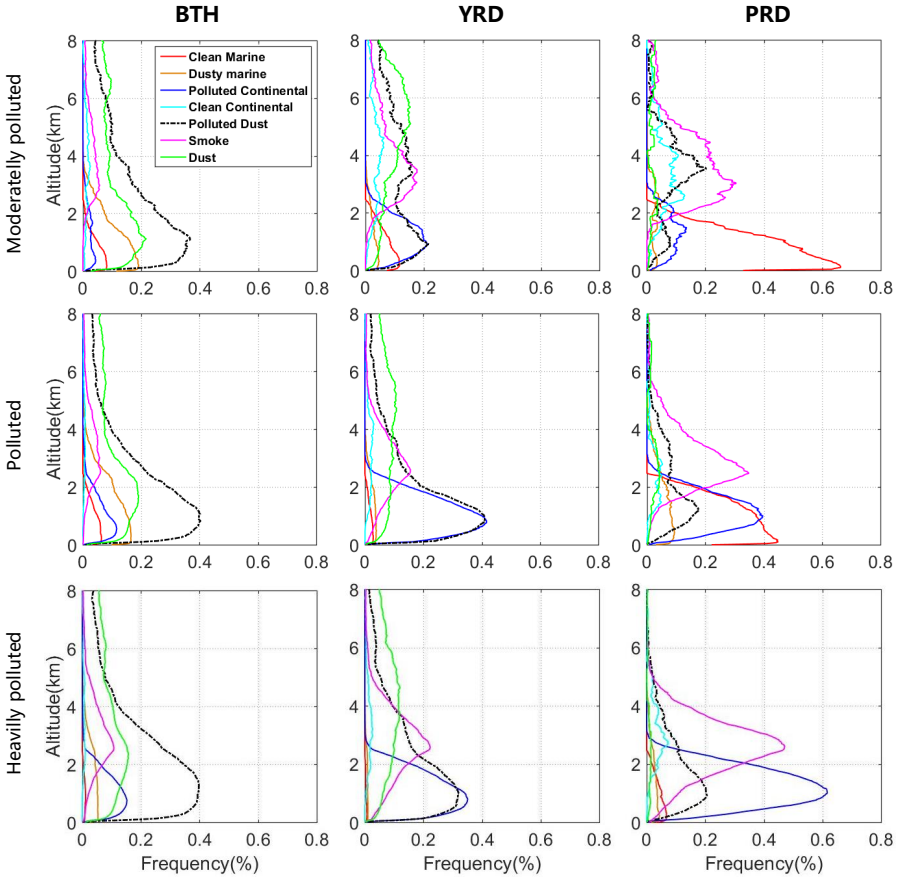

Figure 6 Vertical distribution of the FO of different CALIOP aerosol types, grouped in different CALIOP AOD ranges as indicated by moderately polluted (top), polluted (middle) and heavily polluted (bottom), over the BTH (left), YRD (middle) and PRD (right), averaged over the years 2007-2015.

3.4 Vertical distributions of aerosol types during different meteorological conditions

Many studies show the strong effects of local meteorological conditions on the occurrence of air pollution and the formation of haze (Sun et al., 2015; Shen et al., 2020; Lakshmi et al., 2020). However, most previous studies focused on the influence of meteorological conditions on AOD and aerosol concentration (He et al., 2008; Qiu et al., 2011; Tian et al., 2017). In this study, the focus is on aerosol types and their vertical distributions. The observations over the YRD are selected as an example to illustrate effects of local meteorological conditions (RH and BL thermodynamics) on the aerosol vertical distribution during nighttime.

3.4.1 Influence of relative humidity on the vertical distributions of aerosol types over the YRD

To investigate the influence of relative humidity on the vertical distribution of the aerosol types over the YRD, the profiles were divided into three equally sized subsets with increasing RH at 950 hPa. The

https://doi.org/10.5194/acp-2020-1278
Preprint. Discussion started: 19 January 2021

Atmospheric Chemistry and Physics Discussions

mean RH values for each subset are 47.5% (0 to 66%), 76.9% (66% to 86%) and 93.8% (86% to 100%). The averaged vertical profiles of the FO of different aerosol types in each RH subset are presented in Fig. 7.

As discussed above, the four most prominent aerosol types over the YRD are polluted continental in layer B), polluted dust (layers B and C), smoke (layer C) and dust (over the whole layer). The behaviour of the FOs of the first three types is contrasting. Where polluted dust dominates at low RH, the FO of the polluted dust in layer B decreases strongly with increasing RH while in layer C the FO does not change much. In contrast, the FO of the polluted continental type is highest at intermediate RH, while at the highest RH it is similar to that at low RH and layer B is deeper at the highest RH. The FO of smoke increases with increasing RH and layer C is deepest at the highest RH. The FO of dust is distributed across the vertical, with the highest values in layers A and B at low RH, and negligible FO at the two higher RH situations. During the latter, dust is mainly detected at higher altitudes.

These differences indicate that the occurrence and changes in the FO during different RH conditions are related to different air mass origins, i.e. transport of air masses of different origin with different meteorological conditions. This is particularly indicated by the increase of smoke in layer 3, and the greater FO of dust at higher altitudes in the two higher RH conditions: both these observations indicate long range transport.

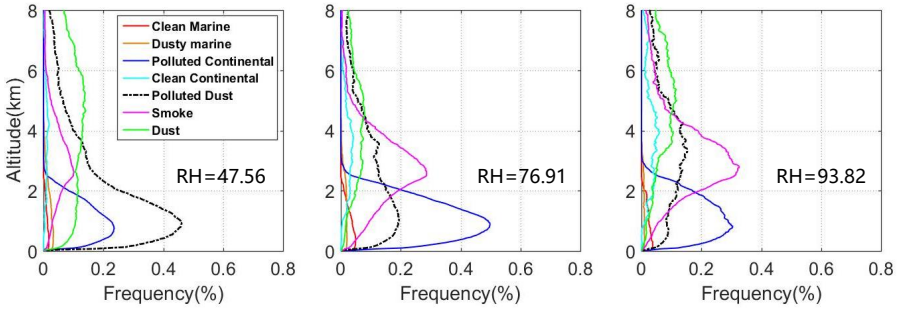

Figure 7 Vertical distributions of the FO of different aerosol types for data stratified by RH; low RH (left, %), intermediate RH (middle, %) and high RH (right, %) over the YRD, averaged over the years 2007-2015.

3.4.2 Influence of BL thermodynamics and dynamics on the vertical distributions of aerosol types over the YRD

The occurrence of aerosol depends on local sources, i.e. direct production and secondary formation from precursor gases, and processes affecting their transformation and dispersion, as well as long-range transport from remote sources. Atmospheric circulation and the resulting weather conditions affect the formation and transformation of aerosol particles (Zhang et al., 2008; Cao et al., 2013). The pressure vertical velocity (PVV) is a measure of dynamic convection strength, i.e. vertical mixing. As shown above, aerosol particles mainly occur at heights from near the surface to 4 km, so the PVV at 750 hPa (about 2.4 km) could be used to characterize the atmospheric dynamic conditions. A negative PVV is indicative of ascending air masses and a positive PVV indicates descending air masses (Jones et al., 2009). Figure 8 shows the mean vertical distribution of the FO of aerosol types stratified by negative and positive PVV. The peak FOs of polluted dust and polluted continental aerosol in layer B are larger

https://doi.org/10.5194/acp-2020-1278
Preprint. Discussion started: 19 January 2021

Atmospheric Chemistry and Physics Discussions

and occur at somewhat lower altitude when PVV>0, indicating that descending motion of air masses is conducive to the deposition and accumulation of aerosols in the lower atmospheric layers (Tian et al., 2017). However, the peak FO of smoke aerosol in layer C is smaller in that situation, which indicates that the PVV mainly affects aerosol in layer B (and possibly A, but that is not clearly visible in the data), i.e. in the mixing layer but not in the free troposphere above. The FO for dust, clean marine and clean continental aerosol in layers A and B are so small that a possible effect of boundary layer dynamics would be too small to observe changes under different PVV conditions.

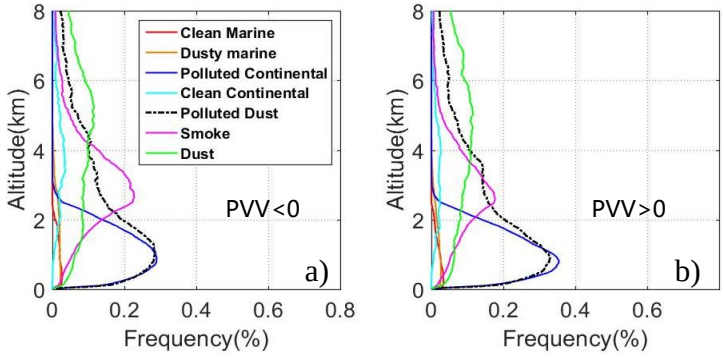

Figure 8 Vertical distributions of the FO of different aerosol types for data stratified by PVV<0 (left) and PVV>0 (right) over the YRD, averaged over the years 2007-2015.

The thermal stability of the atmosphere is closely related to the diffusion and accumulation of aerosols (Kipling et al., 2016). The stability of the lower atmosphere is one of the common atmospheric thermal conditions, which is used to describe the increase or decrease of the vertical motion of the atmosphere. The lower tropospheric stability (LTS) is calculated from the difference of the potential temperature in the free atmosphere (700hPa) and near the surface (1000hPa), indicating a measure of the atmospheric thermodynamic state (Klein and Hartmann, 1993). The larger the LTS, the more stable the atmosphere and the tendency to deter vertical motion; and vice versa, the smaller the LTS, the more unstable the atmosphere and the tendency to facilitate vertical motion. In this study, all aerosol samples were divided into three equally sized subsets from the lowest to the highest LTS. Mean vertical distributions of the FO of the aerosol subtypes, averaged over the years 2007-2015, for each subset are presented in Fig. 9. In unstable atmospheric conditions (LTS=28.93), dust aerosol dominates at altitudes higher than 4 km and polluted dust dominants below 4 km. In contrast, polluted continental is the dominant aerosol type below 2 km and smoke dominates above 2 km during stable atmospheric conditions. Figure 9 also shows that the peak FO of smoke aerosols around 3 km (i.e. in the free troposphere above the atmospheric boundary layer). Due to the heat released by fossil fuel combustion and biomass burning, the temperature near the ground will rise, and the updraft results in the transport of smoke aerosols into the higher atmosphere, i.e. layer C. The data in Fig. 9 show that the FO of polluted continental aerosol in layer B increases when the atmosphere becomes more stable, which indicates that, when turbulence and convection are restrained, aerosol particles tend to accumulate in the near surface layer (Tian et al., 2017). In contrast, the peak FOs of polluted dust and dust aerosol in layer B gradually decreases with the increase of LTS. This may imply that convection can lift dust aerosols to higher altitudes.

https://doi.org/10.5194/acp-2020-1278
Preprint. Discussion started: 19 January 2021

Atmospheric Chemistry and Physics Discussions

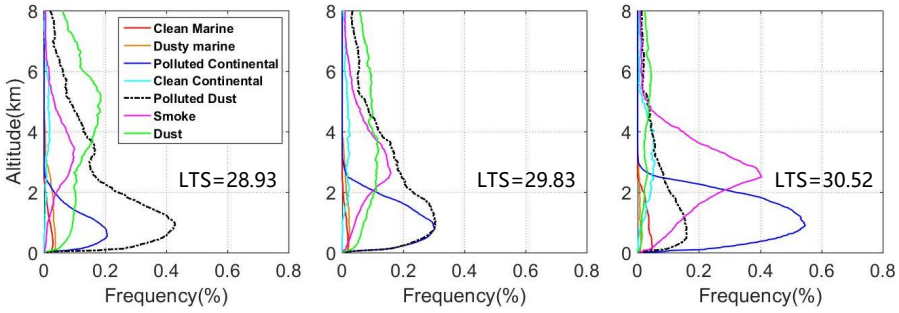

Figure 9 Vertical distributions of the FO of different aerosol types for data stratified by unstable atmosphere (left), neutral stable atmosphere (middle) and stable atmosphere (right) over the YRD, averaged over the years 2007-2015.

3.5 Day/night variation of the vertical distributions of aerosol types

The two CALIPSO overpasses, at 1:30 am and pm local time, provide information on the day/night differences of the vertical distribution of the FO of the aerosol types derived from the CALIOP observations. Figure 10 shows the vertical distributions of the FO of the aerosol types during the daytime overpasses over each of the three regions, for each season averaged over the years 2007-2015. Comparison of the daytime vertical distributions in Fig. 10 with the nighttime vertical distributions in Fig. 5 shows substantial differences which depend on altitude, aerosol type, season and region. To clearly illustrate these differences, difference plots (night – day) are presented in Fig. 11. Fig. 11 shows, for instance, that in the summer, in all three regions, the maximum FO of the polluted dust layers is larger during the day than during the night (negative night-day difference). The difference is much larger over the PRD than over the YRD which in turn is larger than over the BTH. In contrast, for smoke the maximum FO during the day over the PRD and YRD is substantially smaller than during the night (positive night-day difference), while over the BTH the day/night difference is rather small. For clean marine aerosol the FO is larger during the night in the PRD and negligible in the other two regions.

https://doi.org/10.5194/acp-2020-1278
Preprint. Discussion started: 19 January 2021

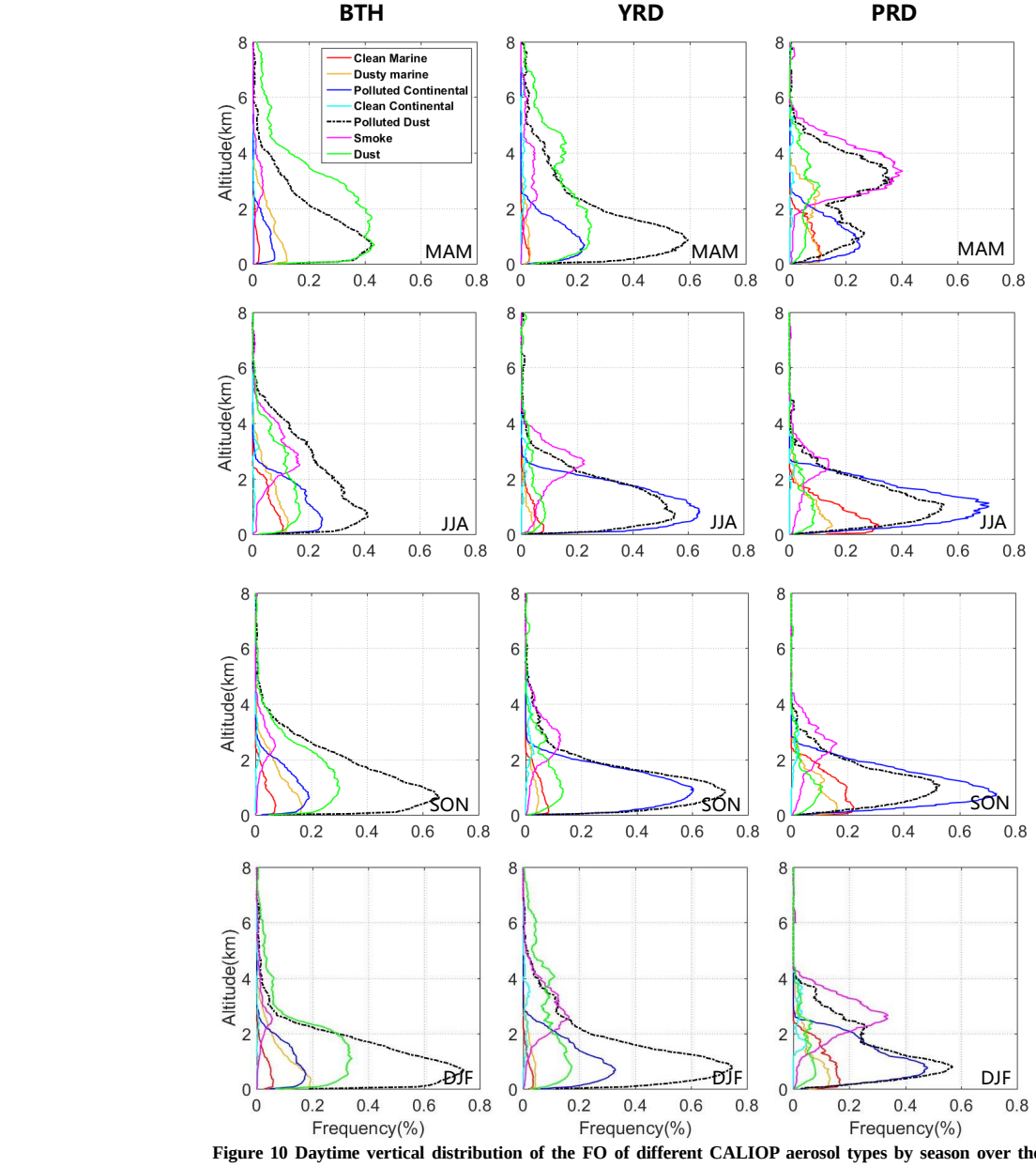

Figure 10 Daytime vertical distribution of the FO of different CALIOP aerosol types by season over the BTH (top), YRD (middle) and PRD (bottom) averaged over the years 2007-2015.

For polluted continental aerosol, however, the difference profiles in Fig. 11 clearly show that the daytime FO is highest in a layer adjacent to the surface (night minus day negative) which is clearly separated from the layer above where the FO is higher during the night. The distribution of polluted continental aerosol over two layers is not evident from either the daytime or the nighttime FO distributions, although a closer look shows some small discontinuities in the vertical distributions. The higher daytime FO indicates the accumulation of this aerosol type in a turbulent mixed layer

https://doi.org/10.5194/acp-2020-1278
Preprint. Discussion started: 19 January 2021


Atmospheric Chemistry and Physics Discussions

which expands under the influence of solar heating. After sunset, radiative cooling of the surface results in the formation of a stable nocturnal boundary attached to the surface which lifts the mixed layer into a disconnected residual layer (Stull, 1988), including the polluted continental aerosol which is thus observed at higher elevation.

This separation is most clearly observed over the PRD during the summer and autumn, although the distribution over two different layers is also suggested by the profiles in winter and spring. The profiles over the YRD in the summer and autumn behave similarly, although weaker than over the PRD. In all these cases, polluted continental is the dominant aerosol type, or one of the most dominant aerosol types, in the lower 2 km. Polluted continental aerosol is emitted, or formed from precursor gases, near the surface and its transport to higher elevations is prohibited by the temperature inversion at the top of the mixed layer. The formation from precursor gases often involves a photo-chemical reaction, i.e. requires the availability of solar radiation and thus occurs during daytime.

In contrast, marine aerosol is directly emitted from the ocean in high wind conditions when waves break (de Leeuw et al., 2011). Marine aerosol is confined to the mixed layer (layer A) and significant FOs of clean marine and dusty marine aerosol are mainly observed over the PRD, in all four seasons. Fig. 11 shows that the FO of dusty marine aerosol is higher during the day than during the night, whereas in contrast, the FO of clean marine aerosol is higher during the night. Over the ocean the air-sea temperature difference does not change strongly as it does over land and thus nocturnal boundary layers are not formed over the ocean. Marine aerosol is transported to the study area, which is over land, in on-shore wind and hence marine aerosol is well distributed over the lower boundary layer.

Dust is long-range transported from the deserts in the north and west of China where it is emitted to high elevations before is passes over the mountains to east China (Proestakis et al., 2018). The day/nighttime difference profiles show a separation at altitudes of 2-4 km, above which the FO of dust is larger during the night while at lower altitudes the dust FO is larger during the day. The altitude depends on the season as is most clearly illustrated from the profiles over the BTH where the dust occurs most frequently: the separation is at about 4 km in the spring and summer, ~3 km in the autumn and ~2.5 km in the winter. Clearly, the dust aerosol is transported from above to the lower layers where it mixes with pollution to form polluted dust. This is probably the reason for the different day/night behaviour of polluted dust and polluted continental aerosol. The concentrations of clean continental aerosol are too small to discuss in terms of day/night differences, except over the PRD in the summer and autumn where it is observed in layer C and behaves similar to smoke aerosol, i.e. the FO is higher during the night than during the day.

https://doi.org/10.5194/acp-2020-1278
Preprint. Discussion started: 19 January 2021

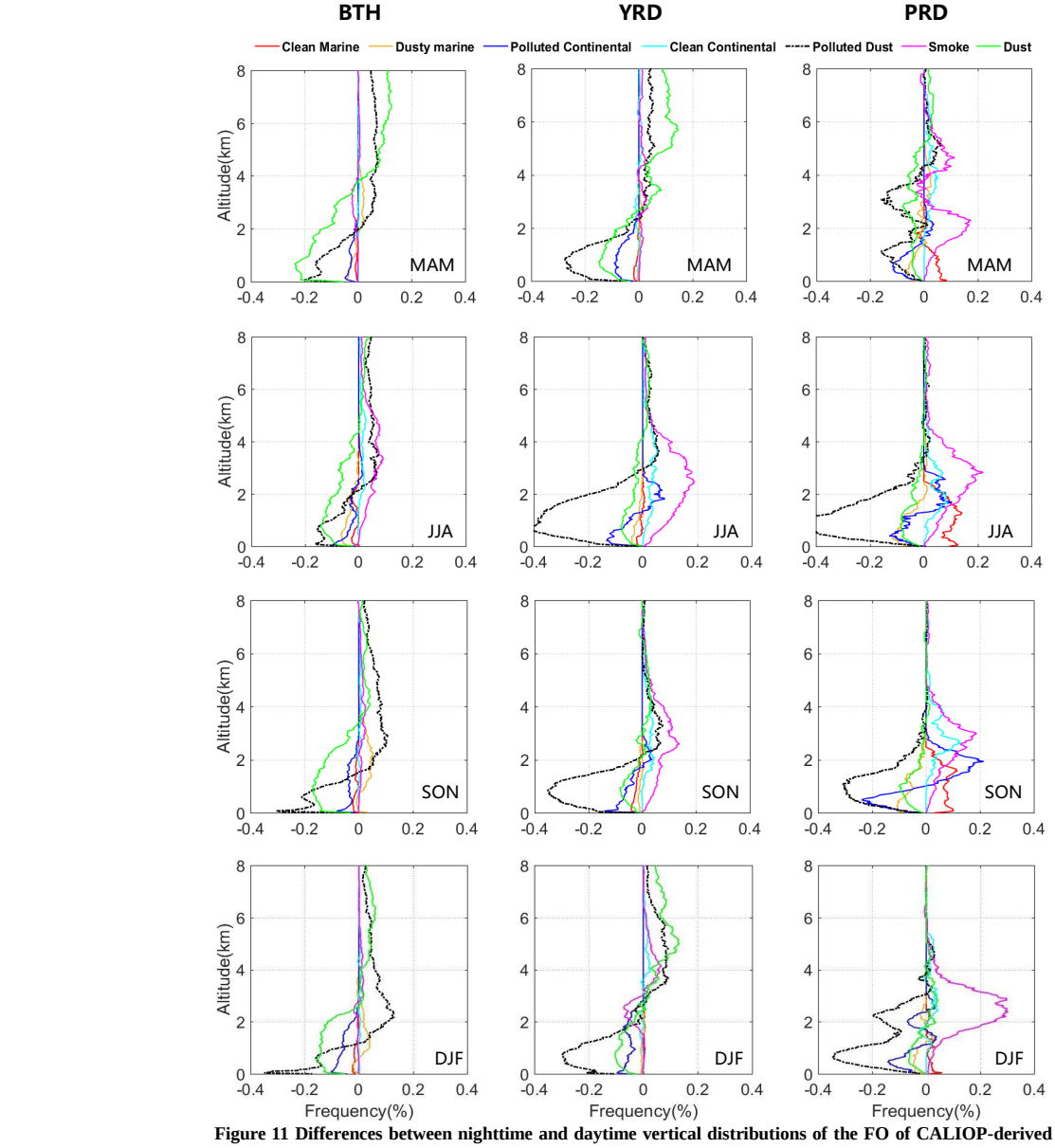

Figure 11 Differences between nighttime and daytime vertical distributions of the FO of CALIOP-derived aerosol types (nighttime minus daytime measurements) by season over the BTH (top), YRD (middle) and PRD (bottom) averaged over the years 2007-2015.

3.6 Discussion

Based on the above findings, the regional and seasonal variations of the spatial and vertical distributions of aerosol properties are discussed in the following.

https://doi.org/10.5194/acp-2020-1278
Preprint. Discussion started: 19 January 2021

Atmospheric Chemistry and Physics Discussions

- In the summer, the AOD is highest over the BTH and YRD (Fig. 1b), which may be attributable to more abundant water vapor and higher temperatures in the summer resulting in strong convection causing deeper boundary layers. The moist air results in higher RH and thus in the swelling of aerosol particles, i.e. a shift of the particle size distribution to larger sizes which in turn results in higher extinction and AOD. The higher temperature results in faster chemical reactions and thus formation of secondary aerosol. With the increased RH, the peak FOs of smoke and clean continental aerosol increase and the peak FO of polluted continental aerosol reaches its maximum value under humid conditions (Fig. 7). Dynamically, the altitude of the peak FO of smoke increases when the ascending motion of air masses occurs (Fig. 9). In addition, biomass burning is the main source of smoke aerosol in the summer. This is in line with smoke aerosol being the second dominant aerosol type above 2 km over the BTH in the summer. Over the YRD, smoke is the dominant aerosol type above 2 km during the summer (Fig. 5). In contrast, the AOD is lowest over the PRD, which may be due to wet removal by East Asian summer monsoon precipitation. Fig. 5 also shows that the FO of clean marine aerosol over the PRD is highest in the summer. Moreover, polluted continental aerosol dominates the aerosol below 3 km over the YRD and PRD in the summer.
- In the spring, the AOD is highest over the PRD (Fig. 1b), which may be related to long-range transport of pollutants from biomass burning in southeast Asia. This is consistent with the observation that smoke is the dominant aerosol type above 2 km and the FO extends to higher altitudes than in other seasons (Fig. 5). Over the BTH and YRD, dust and polluted dust dominate from near the surface to the upper troposphere, leading to the higher AOD over these two areas. Over the YRD, the altitude of the peak FO of dust in MAM and DJF is substantially higher (5 km) than over the BTH (Fig. 5), which may be due to the long-range transport of dust aerosol by westerly winds from north-west China.
- In the autumn, the AOD over the three regions is relatively low throughout the year (Fig. 1b). In this season, the whole eastern region is dominated by westerly winds, which transports relatively clean air to the study regions and contributes to the diffusion of aerosols. The impact of dust storms is relatively small in the autumn.
- In the winter, the prevailing northerly wind brings dry and clean air to the study regions and hence the aerosol concentrations, and thus AOD, are low (Qi et al., 2013; Si et al., 2018). Nevertheless, high AOD does occur frequently in the winter, which is reflected in the average AOD of 0.7 over the BTH in February. Very high values occur during weather conditions conducive of the formation of haze (low wind speed, low BLH, stable stratification). The peak FOs of smoke, polluted continental and clean continental aerosol get larger and that of dust and polluted dust aerosol gets smaller when the atmosphere become stable (Fig. 9).
- With regard to the altitude of the peak FOs of the aerosol types over the three regions, the order from low to high altitude is overall as follows: dust > polluted dust > clean continental/smoke > polluted continental > clean marine/dusty marine.

https://doi.org/10.5194/acp-2020-1278
Preprint. Discussion started: 19 January 2021

Atmospheric Chemistry and Physics Discussions

4 Conclusions

The four dimensional (time scales from yearly to monthly, horizontal and vertical) variations of aerosol properties over three major urban clusters in eastern China have been investigated using satellite observations by passive (MODIS/Aqua) and active (CALIOP/CALIPSO) instruments, both flying on the Aqua satellite, together with ERA Interim Reanalysis meteorological data, for the years 2007-2015. Three areas, BTH, YRD and PRD have been selected because of the diverse natural and anthropogenic aerosol sources as well as different climatic characteristics, providing a unique natural laboratory for the investigation of aerosol properties.

On the inter-annual scale, the highest average AOD occurs in 2011 over the YRD, and the highest AOD over the BTH and PRD are lower and occur in 2012. After 2011 and 2012, respectively, the AOD shows a decreasing trend as also observed in other studies (de Leeuw et al., 2018; Sogacheva et al, 2018). Between 2007 and 2015, the average AOD over the three representative regions decreased overall. On a seasonal scale, the AOD over the BTH peaks in the summer, whereas over the YRD and the PRD the AOD peak occurs in the spring. On a monthly scale, the summer AOD peak over the BTH occurs in July (0.86), whereas over the YRD it clearly occurs in June (0.93). In contrast, over the PRD the AOD peaks in March (0.78), with a weaker maximum in October (0.54); much lower AOD values occur in the summer and a clear minimum in July. Regarding the AOD spatial distribution in three regions, the AOD over the BTH is high in the Southeast over Hebei and Shandong and low over the mountains in Shanxi province in the Northwest. The AOD over the YRD is lower over the Zhejiang and southern Anhui provinces as compared to other areas during the whole year. Over the PRD, the AOD spatial distribution shows a ring-shaped declining pattern, with the highest values in the inner ring and decreasing toward the outer ring.

Comparing the aerosol types in the three urban clusters, the contributions of clean ocean, polluted continental, clean continental and smoke aerosol were the lowest over the BTH, while over the PRD they were highest. In contrast, the contributions of polluted dust and dust aerosol over the BTH dominated the aerosol composition, while over the PRD the contributions of these types were the lowest. The altitude dependence of the vertical frequencies of occurrence of aerosol layers was also investigated. Over the BTH, the top two dominating aerosol types from the altitude of 1.8 km to as high as 8 km are dust and polluted dust in all seasons, except for the summer. Smoke is the second dominant aerosol type above 2 km and polluted continental is the second dominant aerosol type below 2 km in the summer. Over the YRD, dust is detected from near the surface to the upper troposphere and the altitude of the peak FO is about 5 km in the spring and winter. Smoke aerosols dominate from 2 km to 5 km in the summer and autumn, while polluted continental aerosol is dominant below 2 km. Over the PRD, smoke is the dominant aerosol type above ~ 2 km in all seasons and clean marine aerosol is the second most frequently observed aerosol type below ~ 2 km in the summer and autumn. Moreover, polluted continental aerosol in the three target regions is always observed close to the ground in all seasons. In addition, the FOs of polluted continental and clean marine aerosol are larger over the PRD than over the BTH and YRD.

The change of the distribution of the frequency of occurrence of the aerosol types with increasing AOD shows that the peak FOs of clean continental aerosols and clean marine aerosols gradually decrease

https://doi.org/10.5194/acp-2020-1278
Preprint. Discussion started: 19 January 2021

Atmospheric Chemistry and Physics Discussions

with increasing AOD in the three regions. In heavily polluted conditions, the peak FO of smoke aerosol at an altitude of ~ 2.5 km is largest over the three regions. The FOs of smoke and dust aerosol in low AOD conditions occur at higher altitude than during the other two AOD conditions. The extinction coefficient of the aerosols below 6 km is lowest over the PRD and highest over the YRD.

The variation of the aerosol vertical distribution was also analysed in terms of relative humidity and dynamic and thermodynamic boundary layer conditions. Overall, the FOs of clean continental and smoke aerosol gradually increase with the increase of RH. In addition, the altitude of the peak FO of smoke aerosol is largest during conditions with high relative humidity. Dynamically, the downward motion of air parcels can increase the FOs of polluted dust and polluted continental aerosol at 1 km. With regard to thermal stability and vertical mixing, using LTS as a proxy, the peak FOs of smoke and polluted continental aerosol increase when the atmosphere becomes more stable. Conversely, the peak FOs of polluted dust and dust aerosol around 1 km gradually decrease with the increase of LTS.

In this study, nighttime CALIOP observations were used to study the vertical distribution of aerosol types and extinction coefficients. During the night, meteorological conditions, atmospheric chemistry and aerosol processes are different from those during the day. The two CALIPSO overpasses, at 1:30 am and pm local time, were used to evaluate daytime/nighttime differences between the vertical distributions of the frequency of occurrence of CALIOP-derived aerosol types. These differences depend on the aerosol type, altitude, season and location and provide information on effects of aerosol transport and boundary layer processes on the vertical distribution of different aerosol types.

In summary, the aerosol properties, aerosol types and vertical profiles in different AOD and meteorological conditions over three representative regions over eastern China were described, using synergetic use of aerosol products from active and passive sensors. This work can be used to improve model assessment of the direct and indirect aerosol effects in eastern China (Wang et al., 2011; Wu et al., 2016).

Data availability

All data used in this study are publicly available. The satellite data from the MODIS instrument used in this study were obtained from https:// ladsweb.modaps.eosdis.nasa.gov/search/ (last access: 19 January 2021). All data used in this study are publicly available. The satellite data from the CALIOP instrument used in this study were obtained from https://subset.larc.nasa.gov/calipso/ (last access: 19 January 2021). The ECMWF ERA-Interim data were collected from the ECMWF data server http://apps.ecmwf.int/datasets/data/interim-full-daily/levtype=pl/ (last access: 19 January 2021).

Author contributions

YL and TL designed the research. YL led the analyses. YL and GL wrote the manuscript with major input from JH and further input from all other authors. All authors contributed to interpreting the results and to the finalization and revision of the manuscript.

https://doi.org/10.5194/acp-2020-1278
Preprint. Discussion started: 19 January 2021

Atmospheric Chemistry and Physics Discussions

Competing interests

The authors declare that they have no conflict of interest.

Acknowledgements

This work was supported by the National Natural Science Foundation of China (Grant No. 42001290), the China Postdoctoral Science Foundation (Grant No. 2018M630733) and the CAS Strategic Priority Research Program (Grant No. XDA19030402). Many thanks are expressed to NASA for making available the MODIS and CALIOP data. We are grateful for the easy access to the daily ERA Interim Reanalysis data provided by ECMWF. We also thank the reviewers of this paper for their valuable comments which helped improve the manuscript.

References

Albrecht, B.A., 1989. Aerosols, cloud microphysics, and fractional cloudiness. Science 245 (4923), 1227.

Andreae, M., Rosenfeld, D., Artaxo, P., Costa, A., Frank, G., Longo, K., Silva-Dias, M., 2004. Smoking rain clouds over the Amazon. Science 303 (5662), 1337-1342.

Andersson, A., Deng, J., Du, K., Zheng, M., Yan, C., Sköld, M., and Gustafsson, O.: Regionally-varying combustion sources of the January 2013 severe haze events over eastern China, Environ. Sci. Technol., 49, 2038–2043, doi:10.1021/es503855e, 2015.

Bauer, S. E., Bausch, A., Nazarenko, L., Tsigaridis, K., Xu, B., Edwards, R., Bisiaux, M., and McConnell, J.: Historical and future black carbon deposition on the three ice caps: ice core measurements and model simulations from 1850 to 2100, J. Geophys. Res., 118, 7948-7961, doi:10.1002/jgrd.50612, 2013.

Bilal, M., Nazeer, M., Nichol, J., Qiu, Z.F., Wang, L.C., Bleiweiss, M.P, Shen, X.J., Campbell, J.R., and Lolli, S.: Evaluation of Terra-MODIS C6 and C6.1 Aerosol Products against Beijing, XiangHe, and Xinglong AERONET Sites in China during 2004-2014, Remote Sens, 11, 486, 2019.

Cao, X., Wang, Z., Tian, P., Wang, J., Zhang, L., and Quan, X.: Statistics of aerosol extinction coefficient profiles and optical depth using lidar measurement over Lanzhou, China since 2005-2008, J. Quant. Spectrosc. Ra., 122, 150-154, doi:10.1016/j.jqsrt.2012.09.016, 2013.

Che, H., Zhang, X.-Y., Xia, X., Goloub, P., Holben, B., Zhao, H., Wang, Y., Zhang, X.-C., Wang, H., Blarel, L., Damiri, B., Zhang, R., Deng, X., Ma, Y., Wang, T., Geng, F., Qi, B., Zhu, J., Yu, J., Chen, Q., and Shi, G.: Ground-based aerosol climatology of China: aerosol optical depths from the China Aerosol Remote Sensing Network (CARSNET) 2002-2013, Atmos. Chem. Phys., 15, 7619-7652, https://doi.org/10.5194/acp-15-7619-2015, 2015.

Che et al. (2019). Long-term validation of MODIS C6 and C6.1 Dark Target aerosolproducts over China using CARSNET and AERONET. Chemosphere 236 (2019) 12426. https://doi.org/10.1016/j.chemosphere.2019.06.238 00.

https://doi.org/10.5194/acp-2020-1278
Preprint. Discussion started: 19 January 2021

Chen, J.S., Xin, J.Y., An, J.L., Wang, Y.S., Liu, Z.R., Chao, N., Meng, Z.: Observation of aerosol optical properties and particulate pollution at background station in the Pearl River Delta region, Atmospheric Research, 143, 216-227, 2014.

Cheng, F., Zha, Y., Zhang, J., He, J. and Yan, S. (2017). A Study on Distance Transport of PM2.5 to Xianlin in Nanjing, China and its Source Areas. Aerosol Air Qual. Res. 17: 1772-1783.

Costantino, L., Bréon, F.M., 2013. Aerosol indirect effect on warm clouds over south-East Atlantic, from co-located MODIS and CALIPSO observations. Atmos. Chem. Phys. 13, 69-88.

Deng, X., Tie, X., Wu, D., Zhou, X., Bi, X., Tan, H., Li, F., and Jiang, C.: Long-term trend of visibility and its characterizations in the Pearl River Delta (PRD) region, China, Atmos. Environ., 42, 1424-1435, https://doi.org/10.1016/j.atmosenv.2007.11.025, 2008.

de Leeuw, G., Sogacheva, L., Rodriguez, E., Kourtidis, K., Georgoulias, A.K., Alexandri, G., Amiridis, V., Proestakis, E., Marinou, E., Xue, Y., van der A, R., 2018. Two decades of satellite observations of AOD over mainland China using ATSR-2, AATSR and MODIS_Terra_ data set evaluation and large-scale patterns, Atmos. Chem. Phys., 18, 1573-1592, https://doi.org/10.5194/acp-18-1573-2018.

Dong, Z., Li, Z., Yu, X., Cribb, M., Li, X., and Dai, J.: Opposite long-term trends in aerosols between low and high altitudes: a testimony to the aerosol-PBL feedback, Atmos. Chem. Phys., 17, 7997-8009, https://doi.org/10.5194/acp-17-7997-2017, 2017.

Guo, J., Liu, H., Wang, F., Huang, J., Xia, F., Lou, M., Wu, Y., Jiang, J. H., Xie, T., Zhaxi, Y., and Yung, Y. L.: Three dimensional structure of aerosol in China: a perspective from multi-satellite observations, Atmos. Res., 178-179, 580-589, 2016a.

Guo, J.P., Miao, Y.C., Zhang, Y., Liu, H., Li, Z.Q., Zhang, W.C., He, J., Lou, M.Y., Yan, Y., Bian, L.G., Zhai, P.M.: The climatology of planetary boundary layer height in China derived from radiosonde and reanalysis data, Atmos. Chem. Phys., 16, 13309-13319, https:// doi:10.5194/acp-16-13309-2016, 2016b.

Guo, J.P., Liu, H., Li, Z.Q., Rosenfeld, D., Jiang, M.J., Xu, W.X., Jiang, J.H., He, J., Chen, D.D., Min, M., Zhai, P.M.: Aerosol-induced changes in the vertical structure of precipitation: a perspective of TRMM precipitation radar, Atmos. Chem. Phys., 18, 13329-13343, https://doi.org/10.5194/acp-18-13329-2018, 2018.

He, Q. S., Li, C. C., Mao, J. T., Lau, A. K. H., and Chu, D. A.: Analysis of aerosol vertical distribution and variability in Hong Kong, J. Geophys. Res., 113, D14211, doi:10.1029/2008JD009778, 2008.

Heese, B., Baars, H., Bohlmann, S., Althausen, D., Deng, R., 2017. Continuous vertical aerosol profiling with a multi-wavelength Raman polarization lidar over the Pearl River Delta, China. Atmos. Chem. Phys., 17, 6679-6691, doi:10.5194/acp-17-6679-2017.

He, Q., Ming, Z., and Huang, B.: Spatio-temporal variation and impact factors analysis of satellite based aerosol optical depth over China from 2002 to 2015, Atmos. Environ., 129, 79-90, 2016.

He, L.J., Wang, L.C., Lin, A.W., Zhang, M., Xia, X.A., Tao, M.H., Zhou, H., 2018. What drives changes in aerosol properties over the Yangtze River Basin in past four decades? Atmos. Environ. 190, 269-283.

Hou, X.W., Zhu, B., Kumar, K.R., Lu, W., 2019. Inter-annual variability in fine particulate matter pollution over China during 2013-2018_ Role of meteorology. Atmos. Environ. 214, 116842.

Hou, X., Zhu, B., Kumar, K. R., deLeeuw, G., Lu, W., Huang, Q., & Zhu, X.(2020). Establishment of conceptualschemas of surface synopticmeteorological situations affectingfineparticulate pollution across

https://doi.org/10.5194/acp-2020-1278
Preprint. Discussion started: 19 January 2021

eastern China in the winter. Journal of Geophysical Research: Atmospheres, 125, e2020JD033153. https://doi.org/10.1029/2020JD033153.

Hsu, N. C., Tsay, S. C., King, M. D., and Herman, J. R.: Aerosol properties over bright-reflecting source regions, IEEE T. Geosci. Remote, 42, 557–569, https://doi.org/10.1109/TGRS.2004.824067, 2004.

Hsu, N. C., Gautam, R., Sayer, A. M., Bettenhausen, C., Li, C., Jeong, M. J., Tsay, S.-C., and Holben, B. N.: Global and regional trends of aerosol optical depth over land and ocean using SeaWiFS measurements from 1997 to 2010, Atmos. Chem. Phys., 12, 8037–8053, https://doi.org/10.5194/acp-12-8037-2012, 2012.

Huang, L., Jiang, J.H., Tackett, J.L., Su, H., Fu, R., 2013. Seasonal and diurnal variations of aerosol extinction profile and type distribution from CALIPSO 5-year observations. Journal of Geophysical research: Atmospheres, vol. 118, 4572-4596, doi: 10.1002/jgrd.50407, 2013.

Huang, J., Huang, Z., Bi, J., Zhang, W., and Zhang, L.: Micro-Pulse Lidar Measurements of Aerosol Vertical Structure over the Loess Plateau, Atmos. Oceanic Sci. Lett., 1, 8-11, doi:10.1080/16742834.2008.11446756, 2008.

IPCC: Climate Change 2013: The Physical Science Basis. Contribution of Working Group I to the Fifth Assessment Report of the Intergovernmental Panel on Climate Change, edited by: Stocker, T. F., Qin, D., Plattner, G.-K., Tignor, M., Allen, S. K., Boschung, J., Nauels, A., Xia, Y., Bex, V., and Midgley, P. M., Cambridge University Press, Cambridge, UK and New York, NY, USA, 1535 pp., 2013.

Jin,Y.,Andersson,H.,andZhang,S.:AirPollutionControlPolicies in China: A Retrospective and Prospects, Int. J. Environ. Res. PublicHealth,13,1219,https://doi.org/10.3390/ijerph13121219, 2016.

Jones, T. A., Christopher, S. A., and Quaas, J.: A six year satellite-based assessment of the regional variations in aerosol indirect effects, Atmos. Chem. Phys., 9, 4091–4114, https://doi.org/10.5194/acp-9-4091-2009, 2009.

Kang, H.Q., Zhu, B., J.van der A, R., Zhu, C.M., de Leeuw, G., 2019. Natural and anthropogenic contributions to long-term variations of SO2, NO2, CO, and AOD over East China. Atmos. Res. 215, 284-293.

Kang, N., Kumar, K.R., Hu, K., Yu, X.N., Yin, Y., 2016. Long-term (2002-2014) evolution and trend in Collection 5.1 Level-2 aerosol products derived from the MODIS and MISR sensors over the Chinese Yangtze River Delta. Atmos. Res. 181, 29-43.

Kaufman, Y. J., Remer, L. A., Tanre, D., Rong-Rong, L., Kleidman, R., Mattoo, S., Levy, R. C., Eck, T. F., Holben, B. N., Ichoku, C., Martins, J. V., and Koren, I.: A critical examination of the residual cloud contamination and diurnal sampling effects on MODIS estimates of aerosol over ocean, IEEE T. Geosci. Remote, 43, 2886-2897, doi:10.1109/TGRS.2005.858430, 2005.

Klein, S. A. and Hartmann, D. L.: The seasonal cycle of low stratiform clouds, J. Climate, 6, 1587–1606, 1993.

Kim, M.H., Omar, A.H., Tackett, J.L., Vaughan, M.A., Winker, D.M., Trepte, C.R., Hu, Y.X., Liu, Z.L., Poole, L.R., Pitts, M.C., Kar, J., and Magill, B.: The CALIPSO Version 4 Automated Aerosol Classification and Lidar Ratio Selection Algorithm, Atmos Meas Tech., 11(11): 6107-6135, 2018.

Kipling, Z., Stier, P., Schwarz, J. P., Perring, A. E., Spackman, J. R., Mann, G. W., Johnson, C. E., and Telford, P. J.: Constraints on aerosol processes in climate models from vertically-resolved aircraft

https://doi.org/10.5194/acp-2020-1278
Preprint. Discussion started: 19 January 2021

observations of black carbon, Atmos. Chem. Phys., 13, 5969-5986, doi:10.5194/acp-13-5969-2013, 2013.

Kipling, Z., Stier, P., Johnson, C. E., Mann, G. W., Bellouin, N., Bauer, S. E., Bergman, T., Chin, M., Diehl, T., Ghan, S. J., Iversen, T., Kirkevåg, A., Kokkola, H., Liu, X., Luo, G., van Noije, T., Pringle, K. J., von Salzen, K., Schulz, M., Seland, Ø., Skeie, R. B., Takemura, T., Tsigaridis, K., and Zhang, K.: What controls the vertical distribution of aerosol? Relationships between process sensitivity in HadGEM3-UKCA and inter-model variation from AeroCom Phase II, Atmos. Chem. Phys., 16, 2221-2241, doi:10.5194/acp-16-2221-2016, 2016.

Koffi, B., et al. (2012), Application of the CALIOP layer product to evaluate the vertical distribution of aerosols estimated by global models: Aerocom phase I results, J. Geophys. Res., 117, D10201, doi:10.1029/2011JD016858

Kourtidis, K., Stathopoulos, S., Georgoulias, A. K., Alexandri, G., and Rapsomanikis, S.: A study of the impact of synoptic weather conditions and water vapor on aerosol–cloud relationships over major urban clusters of China, Atmos. Chem. Phys., 15, 10955-10964, https://doi.org/10.5194/acp-15-10955-2015, 2015.

Kumar, K.R., Yin, Y., Sivakumar, V., Kang, N., Yu, X.N., Diao, Y.W., Adesina, A.J., Reddy, R.R., 2015. Aerosol climatology and discrimination of aerosol types retrieved from MODIS, MISR and OMI over Durban (29.88 degrees S, 31.02 degrees E), South Africa. Atmos. Environ. 117, 9-18.

Lei, Y., Zhang, Q., He, K. B., and Streets, D. G.: Primary anthropogenic aerosol emission trends for China, 1990-2005, Atmos. Chem. Phys., 11, 931-954, https://doi.org/10.5194/acp-11-931-2011, 2011.

Levy, R.C., Mattoo, S., Munchak, L.A., Remer, L.A., Sayer, A.M., Patadia, F., Hsu, N.C., 2013. The Collection 6 MODIS aerosol products over land and ocean. Atmos. Meas. Technol. 6 (11), 2989.

Li, Z., Lau, W. K.-M., Ramanathan, V., Wu, G., Ding, Y., Manoj, M. G., Liu, J., Qian, Y., Li, J., Zhou, T., and Fan, J.: Aerosol and monsoon climate interactions over Asia, Rev. Geophys., 54, 866-929, https://doi.org/10.1002/2015RG000500, 2016.

Li, L. Y., Chen, Y., Xie, S. D.: Spatio-temporal variation of biogenic volatile organic compounds emissions in China [J]. Environmental Pollution, 182(6): 157-168, 2013.

Li, Z., Zhang, Y., Xu, H., Li, K., Dubovik, O., & Goloub, P. (2019). The fundamental aerosol models over China region: A cluster analysis of the ground-based remote sensing measurements of total columnar atmosphere. Geophysical Research Letters, 46, 4924–4932. https://doi.org/10.1029/2019GL082056

Li, Z.Q., Aerosol and Boundary-Layer Interactions and Impact on Air Quality

Lin, J., Nielsen, C. P., Zhao, Y., Lei, Y., Liu, Y., and Mcelroy, B.: Recent changes in particulate air pollution over China observed from space and the ground: effectiveness of emission control, Environ. Sci. Technol., 44, 7771-7776, 2010.

Liu, Z., Vaughan, M., Winker, D., Kittaka, C., Getzewich, B., Kuehn, R., Omar, A.,Powell, K., Trepte, C., and Hostetler, C.: The CALIPSO lidar cloud and aerosol discrimination: Version 2 algorithm and initial assessment of performance, J. Atmos. Ocean. Tech., 26, 1198-1213, 2009.

Liu, X., Yan, L., Yang, P., Yin, Z. Y., North, G. R.: Influence of Indian summer monsoon on aerosol loading in East Asia, J. Appl. Meteorol. Climatol., 50, 523-533, 2011.

https://doi.org/10.5194/acp-2020-1278
Preprint. Discussion started: 19 January 2021

Liu, J. J., Zheng, Y. F., Li, Z. Q., Flynn, C., and Cribb, M.: Seasonal variations of aerosol optical properties, vertical distribution and associated radiative effects in the Yangtze Delta region of China, J. Geophys. Res.-Atmos., 117, D00K38, https://doi.org/10.1029/2011jd016490, 2012.

Liu, Q., Liu, X., Liu, T.Q., Kang, Y.M., Chen, Y.H., Li, J.M., Zhang, H.: Seasonal variation in particle contribution and aerosol types in Shanghai based on satellite data from MODIS and CALIOP, Particuology, 51, 18-25, 2020.

Liu, Y., de Leeuw, G., Kerminen, V.-M., Zhang, J., Zhou, P., Nie, W., Qi, X., Hong, J., Wang, Y., Ding, A., Guo, H., Krüger, O., Kulmala, M., and Petäjä, T.: Analysis of aerosol effects on warm clouds over the Yangtze River Delta from multi-sensor satellite observations, Atmos. Chem. Phys., 17, 5623-5641, https://doi.org/10.5194/acp-17-5623-2017, 2017.

Liu, Y., Zhang, J., Zhou, P., Lin, T., Hong, J., Shi, L., Yao, F., Wu, J., Guo, H., and de Leeuw, G.: Satellite-based estimate of the variability of warm cloud properties associated with aerosol and meteorological conditions, Atmos. Chem. Phys., 18, 18187-18202, https://doi.org/10.5194/acp-18-18187-2018, 2018.

Lu, Z., Streets, D. G., Zhang, Q., Wang, S., Carmichael, G. R., Cheng, Y. F., Wei, C., Chin, M., Diehl, T., and Tan, Q.: Sulfur dioxide emissions in China and sulfur trends in East Asia since 2000, Atmos. Chem. Phys., 10, 6311-6331, https://doi.org/10.5194/acp-10-6311-2010, 2010.

Luo, Y.X., Zheng, X.B., Zhao, T.L., Chen, J., 2014. A climatology of aerosol optical depth over China from recent 10 years of MODIS remote sensing data. Int. J. Climatol. 34: 863-870.

Ma, Z., Hu, X., Sayer, A. M., Levy, R., Zhang, Q., Xue, Y., Tong, S., Bi, J., Huang, L., and Liu, Y.: Satellitebased spatiotemporal trends in PM2:5 concentrations: China, 2004-2013, Environ. Health Persp., 124, 184-192, https://doi.org/10.1289/ehp.1409481, 2016.

Massie, S. T., Delanoë, J., Bardeen, C. G., Jiang, J. H., and Huang, L.: Changes in the shape of cloud ice water content vertical structure due to aerosol variations, Atmos. Chem. Phys., 16, 6091-6105, https://doi.org/10.5194/acp-16-6091-2016, 2016.

Matthias, V., Balis, D., Bosenberg, J., Eixmann, R., Iarlori, M., Komguem, L., Mattis, I., Papayannis, A., Pappalardo, G., Perrone, M. R., and Wang, X.: Vertical aerosol distribution over Europe: Statistical analysis of Raman lidar data from 10 European Aerosol Research Lidar Network (EARLINET) stations, J. Geophys. Res.-Atmos., 109, D18201, https://doi.org/10.1029/2004jd004638, 2004.

Mai, B., Deng, X., Xia, X., Che, H., Guo, J., Liu, X., Zhu, J., Ling, C.: Column-integrated aerosol optical properties of coarse- and fine-mode particles over the Pearl River Delta region in China, Science of the Total Environment, 622-623, 481-492, 2018.

Pan, H.L., Wang, M.Z., Kumar, K.R., Lu, H., Mamtimin, A., Huo, W., Yang, X.H., Yang, F., Zhou, C.L., 2019. Seasonal and vertical distributions of aerosol type extinction coefficients with an emphasis on the impact of dust aerosol on the microphysical properties of cirrus, Atmos. Environ. 203, 216-227.

Petäjä, T., Järvi, L., Kerminen, V.M., Ding, A.J., Sun, J.N., Nie, W., Kujansuu, J., Virkkula, A., Yang, X.Q., Fu, C.B., Zilitinkevich, S., Kulmala, M.: Enhanced air pollution via aerosolboundary layer feedback in China, Scienfic Reports, 6, 18998, 2016.

Proestakis, E., Amiridis, V., Marinou, E., Georgoulias, A. K., Solomos, S., Kazadzis, S., Chimot, J., Che, H., Alexandri, G., Binietoglou, I., Daskalopoulou, V., Kourtidis, K. A., de Leeuw, G., and van der A, R.

https://doi.org/10.5194/acp-2020-1278
Preprint. Discussion started: 19 January 2021

J.: Nine-year spatial and temporal evolution of desert dust aerosols over South and East Asia as revealed by CALIOP, Atmos. Chem. Phys., 18, 1337-1362, https://doi.org/10.5194/acp-18-1337-2018, 2018.

Qi, Y.L., Ge, J.M., Huang, J.P., 2013. Spatial and temperal distribution of MODIS and MISR aerosol optical depth over norther China and comparison with AERONET. Chinese Science Bulletin, 58(20), 2497-2506.

Qiu, C. and Zhang, R.: Multiphase chemistry of atmospheric amines, Phys. Chem. Chem. Phys., 15, 5738-5752, doi:10.1039/C3CP43446J, 2013.

Qiu, Q., Wang, L., Lal, V., Khalizov, A. F., and Zhang, R.: Heterogeneous chemistry of alkylamines on ammonium sulfate and ammonium bisulfate, Environ. Sci. Technol., 45, 4748-4755, doi:10.1021/es1043112, 2011.

Remer, L. A., Kaufman, Y. J., Tanre, D., Mattoo, S., Chu, D. A., Martins, J. V., Li, R. R., Ichoku, C., Levy, R. C., Kleidman, R. G., Eck, T. F., Vermote, E., and Holben, B. N.: The MODIS aerosol algorithm, products, and validation, J. Atmos. Sci., 62, 947-973, doi:10.1175/JAS3385.1, 2005.

Rosenfeld, D., Lohmann, U., Raga, G.B., O'Dowd, C.D., Kulmala, M., Fuzzi, S., Reissell, A., Andreae, M.O., 2008. Flood or drought: how do aerosols affect precipitation? Science 321 (5894), 1309.

Rosenfeld, D., M. O. Andreae, A. Asmi, M. Chin, G. de Leeuw, D. Donovan, R. Kahn, S. Kinne, N. Kivekäs, M. Kulmala, W. Lau, S. Schmidt, T. Suni, T. Wagner, M. Wild, J. Quaas (2014). Global observations of aerosol-cloud-precipitation-climate interactions, Rev. Geophys., 52, 750–808, *doi:*10.1002/2013RG000441.

Samset, B. H., Myhre, G., Herber, A., Kondo, Y., Li, S.-M., Moteki, N., Koike, M., Oshima, N., Schwarz, J. P., Balkanski, Y., Bauer, S. E., Bellouin, N., Berntsen, T. K., Bian, H., Chin, M., Diehl, T., Easter, R. C., Ghan, S. J., Iversen, T., Kirkevåg, A., Lamarque, J.-F., Lin, G., Liu, X., Penner, J. E., Schulz, M., Seland, Ø., Skeie, R. B., Stier, P., Takemura, T., Tsigaridis, K., and Zhang, K.: Modelled black carbon radiative forcing and atmospheric lifetime in AeroCom Phase II constrained by aircraft observations, Atmos. Chem. Phys., 14, 12465-12477, doi:10.5194/acp-14-12465-2014, 2014.

Saponaro, G., Kolmonen, P., Sogacheva, L., Rodriguez, E., Virtanen, T., and de Leeuw, G.: Estimates of the aerosol indirect effect over the Baltic Sea region derived from 12 years of MODIS observations, Atmos. Chem. Phys., 17, 3133-3143, doi:10.5194/acp-17-3133-2017, 2017.

Sayer, A. M., Hsu, N. C., Bettenhausen, C., and Jeong, M. J.: Validation and uncertainty estimates for MODIS Collection 6 “deep Blue” aerosol data, J. Geophys. Res.-Atmos., 118, 7864–7872, https://doi.org/10.1002/jgrd.50600, 2013.

Sayer, A. M., Munchak, L. A., Hsu, N. C., Levy, R. C., Bettenhausen, C., and Jeong, M.-J.: MODIS Collection 6 aerosol products: comparison between Aqua’s e-Deep Blue, Dark Target, and “merged” data sets, and usage recommendations, J. Geophys. Res.-Atmos., 119, 13965–13989, https://doi.org/10.1002/2014JD022453, 2014.

Schwarz, J. P., Spackman, J. R., Gao, R. S., Watts, L. A., Stier, P., Schulz, M., Davis, S. M., Wofsy, S. C., and Fahey, D. W.: Global-scale black carbon profiles observed in the remote atmosphere and compared to models, Geophys. Res. Lett., 37, L18812, doi:10.1029/2010GL044372, 2010.

Seinfeld, J.H., and Pandis, S.N. Atmopsheric Chemistry and Physics: from Air Pollution to Cllimate Change. John Wiley & Sons, New York, 1998. OSBN 0-471-17816-0.

https://doi.org/10.5194/acp-2020-1278
Preprint. Discussion started: 19 January 2021

Seinfeld et al. (2016). Improving our fundamental understanding of the role of aerosol−cloud interactions in the climate system. PNAS May 24, 2016 113 (21) 5781-5790; https://doi.org/10.1073/pnas.1514043113.

Shindell, D. T., Faluvegi, G., Koch, D. M., Schmidt, G. A., Unger, N., and Bauer, S. E.: Improved Attribution of Climate Forcing to Emissions, Science, 326, 716-718, https://doi.org/10.1126/science.1174760, 2009.

Shi, G.M., Liu, R.L., Wang, D.Y., Yang, F.M., 2017. Evaluation of the MODIS C6 aerosol optical depth products over Chongqing, China [J]. Atmosphere, 8(11): 227.

Si, Y., Wang, H.M., Cai, K., Chen, L.F., Zhou, Z.C., Li, S.S., 2019. Long-term (2006-2015) variations and relations of multiple atmospheric pollutants based on multi-remote sensing data over the North China Plain. Environ. Pollut. 255, 113323.

Small, J. D., Jiang, J. H., Su, H., and Zhai, C.: Relationship between aerosol and cloud fraction over Australia, Geophys. Res. Lett., 38, L23802, doi:10.1029/2011GL049404, 2011.

Sogacheva, L., de Leeuw, G., Rodriguez, E., Kolmonen, P., Georgoulias, A. K., Alexandri, G., Kourtidis, K., Proestakis, E., Marinou, E., Amiridis, V., Xue, Y., van der A, R.J.: Spatial and seasonal variations of aerosols over China from two decades of multi-satellite observations – Part 1: ATSR (1995-2011) and MODIS C6.1 (2000-2017), Atmos. Chem. Phys., 18, 11389-11407, https://doi.org/10.5194/acp-18-11389-2018, 2018a.

Sogacheva, L., Rodriguez, E., Kolmonen, P., Virtanen, T. H., Saponaro, G., de Leeuw, G., Georgoulias, A. K., Alexandri, G., Kourtidis, K., and van der A, R. J.: Spatial and seasonal variations of aerosols over China from two decades of multi-satellite observations – Part 2: AOD time series for 1995–2017 combined from ATSR ADV and MODIS C6.1 and AOD tendency estimations, Atmos. Chem. Phys., 18, 16631-16652, https://doi.org/10.5194/acp-18-16631-2018, 2018b.

Sogacheva, L., Popp, T., Sayer, A. M., Dubovik, O., Garay, M. J., Heckel, A., Hsu, N. C., Jethva, H., Kahn, R. A., Kolmonen, P., Kosmale, M., de Leeuw, G., Levy, R. C., Litvinov, P., Lyapustin, A., North, P., Torres, O., and Arola, A.: Merging regional and global aerosol optical depth records from major available satellite products, Atmos. Chem. Phys., 20, 2031–2056, https://doi.org/10.5194/acp-20-2031-2020, 2020.

Song, C.-K., Ho, C.-H., Park, R. J., Choi, Y.-S., Kim, J. Gong, D.-Y., and Lee, Y.-B.: Spatial and seasonal variations of surface PM10 concentration and MODIS Aerosol Optical Depth over China, Asia-Pac. J. Atmos. Sci., 45, 1, 33-43, 2009.

Streets, D. G., Bond, T. C., Carmichael, G. R., Fernandes, S. D., Fu, Q., He, D., Klimont, Z., Nelson, S. M., Tsai, N. Y., Wang, M. Q., Woo, J. H., and Yarber, K. F.: An inventory of gaseous and primary aerosol emissions in Asia in the year 2000, J. Geophys. Res.-Atmos., 108, 8809, https://doi.org/10.1029/2002JD003093, 2003.

Streets, D. G., Yu, C., Wu, Y., Chin, M., Zhao, Z. C., Hayasaka, T., and Shi, G. Y.: Aerosol trends over China, 1980–2000, Atmos. Res., 88, 174-182, 2008.

Stephens, G., Vane, D. G., Boain, R. J., Mace, G. G., Sassen, K., Wang, Z., Illingworth, A. J., O'Connor, E. J., Rossow, W. B., Durden, S. L., Miller, S. D., Austin, R. T., Benedetti, A., and Mitrescu,

C.: The CloudSat Science Team: The CloudSat mission and the A-Train, B. Am. Meteorol. Soc., 83, 1771-1790, 2002.

Stull, R.B. (1988). An introduction to boundary layer meteorology. Kluwer, Dordrecht, ISBN 90277227694.

Su, X., Cao, J., Li, Z., Lin, M., and Wang, G.: Column-Integrated Aerosol Optical Properties during Summer and Autumn of 2012 in Xi'an, China, Aerosol Air Qual. Res., 14, 850–861, doi:10.4209/aaqr.2013.03.0093, 2014.

Sun, Y.L., Wang, Z.F., Du, W., Zhang, Q., Wang, Q.Q., Fu, P.Q., Pan, X.L., Li, J., Jayne, J., Worsnop, D.R., 2015. Long-term real-time measurements of aerosol particle composition in Beijing, China: seasonal variations, meteorological effects, and source analysis. Atmos. Chem. Phys. 15 (17), 10149–10165. http://dx.doi.org/10.5194/acp-15-10149-2015.

Tan, C. H., Zhao, T. L., Xu, X. F., et al. 2015. Climatic analysis of satellite aerosol data on variations of submicron aerosols over East China [J]. Atmospheric Environment, 123(Part B): 392-398.

Tao, M., L. Chen, Z. Wang, J. Tao, H. Che, X. Wang, and Y. Wang (2015), Comparison and evaluation of the MODIS Collection 6 aerosol data in China, J. Geophys. Res. Atmos., 120, 6992-7005, doi:10.1002/2015JD023360.

Tian, P., Cao, X., Zhang, L., Sun, N., Sun, L., Logan, T., Shi, J., Wang, Y., Ji, Y., Lin, Y., Huang, Z., Zhou, T., Shi, Y., and Zhang, R.: Aerosol vertical distribution and optical properties over China from long-term satellite and groundbased remote sensing, Atmos. Chem. Phys., 17, 2509-2523, https://doi.org/10.5194/acp-17-2509-2017, 2017.

Twomey, S., 1974. Pollution and the planetary albedo. Atmos. Environ. 41, 120-125. http://dx.doi.org/10.1016/j.atmosenv.2007.10.062.

Unger, N., Shindell, D. T., Koch, D. M., and Streets, D. G.: Air pollution radiative forcing from specific emissions sectors at 2030, J. Geophys. Res.-Atmos., 113, D02306, https://doi.org/10.1029/2007jd008683, 2008.

van der A, R. J., Mijling, B., Ding, J., Koukouli, M. E., Liu, F., Li, Q., Mao, H., and Theys, N.: Cleaning up the air: effectiveness of air quality policy for SO2 and NOx emissions in China, Atmos. Chem. Phys., 17, 1775–1789, https://doi.org/10.5194/acp17-1775-2017, 2017

Wang, F., Guo, J., Zhang, J., Huang, J., Min, M., Chen, T., Liu, H., Deng, M., Li, X., 2015. Multisensor quantification of aerosol-induced variability in warm clouds over eastern China. Atmospheric Environment 113 (0), 1-9. http://dx.doi.org/10.1016/j. atmosenv.2015.04.063.

Wang, Y., Xin, J., Li, Z., Wang, S., Wang, P., Hao, W. M., Nordgren, B. L., Chen, H., Wang, L., and Sun, Y.: Seasonal variations in aerosol optical properties over China, J. Geophys. Res., 116, D18209, https://doi.org/10.1029/2010JD015376, 2011a.

Wang, Y., Wan, Q., Meng, W., Liao, F., Tan, H., and Zhang, R.: Long-term impacts of aerosols on precipitation and lightning over the Pearl River Delta megacity area in China, Atmos. Chem. Phys., 11, 12421–12436, doi:10.5194/acp-11-12421-2011, 2011b.

Wang, Q., Jacob, D. J., Spackman, J. R., Perring, A. E., Schwarz, J. P., Moteki, N., Marais, E. A., Ge, C., Wang, J., and Barrett, S. R. H.: Global budget and radiative forcing of black carbon aerosol: Constraints

https://doi.org/10.5194/acp-2020-1278
Preprint. Discussion started: 19 January 2021

Atmospheric Chemistry and Physics Discussions

from pole-to-pole (HIPPO) observations across the Pacific, J. Geophys. Res., 119, 2013JD020824, doi:10.1002/2013JD020824, 2014.

Wang, H., Zhang, L., Cao, X., Zhang, Z., and Liang, J.: A-Train satellite measurements of dust aerosol distributions over northern China, J. Quant. Spectrosc. Ra., 122, 170-179, doi:10.1016/j.jqsrt.2012.08.011, 2013.

Wang, J., de Leeuw, G., Niu, S., and Kang, H. (2019). Contrasting aerosol optical characteristics and source regions during summer and winter pollution episodes in Nanjing, China. Remote Sens. 2019, 11, 1696; doi:10.3390/rs11141696.

Winker, D. M., Pelon, J. R., and McCormick, M. P.: The CALIPSO mission: Spacebornelidar for observation of aerosols and clouds, Proc. SPIE, Lidar Remote Sensing for Industry and Environment Monitoring III, 4893, doi:10.1117/12.466539, 2003.

Winker, D. M., Vaughan, M. A., Omar, A., Hu, Y. X., Powell, K. A., Liu, Z. Y., Hunt, W. H., and Young, S. A.: Overview of the CALIPSO Mission and CALIOP Data Processing Algorithms, J. Atmos. Ocean. Tech., 26, 2310-2323, doi:10.1175/2009JTECHA1281.1, 2009.

Wu, G., Li, Z., Fu, C., Zhang, X., Zhang, R., Zhang, R., Zhou, T., Li, J., Li, J., Zhou, D., Wu, L., Zhou, L., He, B., and Huang, R.: Advances in studying interactions between aerosols and monsoon in China, Sci. China Earth Sci., 59, 1–16, doi:10.1007/s11430-015-5198-z, 2016.

Wu, M., Wu, D., Fan, Q., Wang, B. M., Li, H. W., and Fan, S. J.: Observational studies of the meteorological characteristics associated with poor air quality over the Pearl River Delta in China, Atmos. Chem. Phys., 13, 10755–10766, doi:10.5194/acp-13-10755-2013, 2013.

Xie, G.Q., Wang, M., Pan, J., Zhu, Y., 2019. Spatio-temporal variations and trends of MODIS C6.1 Dark Target and Deep Blue merged aerosol optical depth over China during 2000-2017. Atmos. Environ. 214, 116846.

Xu, X., Qiu, J., Xia, X., Sun, L., and Min, M.: Characteristics of atmospheric aerosol optical depth variation in China during 1993-2012, Atmos. Environ., 119, 82-94, 2015.

Xu, Z., Xue, L. K., Wang, T., Xia, T., Gao, Y., Louie, P. K. K., and Luk, C. W. Y.: Measurements of Peroxyacetyl Nitrate at a Background Site in the Pearl River Delta Region: Production Efficiency and Regional Transport, Aerosol Air Qual. Res., 15, 833-841, doi:10.4209/aaqr.2014.11.0275, 2015.

Yang, X., Zhao, C. F., Zhou, L. J., Wang, Y., and Liu, X. H.: Distinct impact of different types of aerosols on surface solar radiation in China, J. Geophys. Res.-Atmos., 121, 6459-6471, https://doi.org/10.1002/2016jd024938, 2016.

Yumimoto, K., Eguchi, K., Uno, I., Takemura, T., Liu, Z., Shimizu, A., Sugimoto, N., 2009. An elevated large-scale dust veil from the Taklimakan desert: intercontinental transport and three-dimensional structure as captured by CALIPSO and regional and global models. Atmos. Chem. Phys. Discuss. 9 (4), 8545-8558.

Yu, X.N., Lü, R., Liu, C., Yuan, L., Shao, Y.X., Zhu, B., Lei, L., 2017. Seasonal variation of columnar aerosol optical properties and radiative forcing over Beijing, China [J]. Atmospheric Environment, 166: 340-350.

https://doi.org/10.5194/acp-2020-1278
Preprint. Discussion started: 19 January 2021

Atmospheric Chemistry and Physics Discussions

Zhang Y. & Li Z., 2015. Remote sensing of atmospheric fine particulate matter (PM2.5) mass concentration near the ground from satellite observation. Remote Sensing of Environment, 160, 252–262.

Zhang, L. and Li, J. (2019). Variability of Major Aerosol Types in China Classified Using AERONET Measurements. *Remote Sens.* 2019, *11*(20), 2334; https://doi.org/10.3390/rs11202334.

Zhang, J., Reid, J. S., Alfaro-Contreras, R., and Xian, P.: Has China been exporting less particulate air pollution over the past decade?, Geophys. Res. Lett., 44, 2941-2948, https://doi.org/10.1002/2017GL072617, 2017.

Zhang, M., Wang, Y., Ma, Y.Y., Wang, L.C., Gong, W., Liu, B.M., 2018. Spatial distribution and temporal variation of aerosol optical depth and radiative effect in South China and its adjacent area. Atmos. Environ. 188, 120-128.

Zhang, R., Khalizov, A. F., Pagels, J., Zhang, D., Xue, H., and McMurry, P. H.: Variability in morphology, hygroscopicity, and optical properties of soot aerosols during atmospheric processing, P. Natl. Acad. Sci. USA, 105, 10291-10296, doi:10.1073/pnas.0804860105, 2008.

Zhang, Y., Li, Z., Chen, Y., de Leeuw, G., Zhang, C., Xie, Y., and Li, K.: Improved inversion of aerosol components in the atmospheric column from remote sensing data, Atmos. Chem. Phys., 20, 12795–12811, https://doi.org/10.5194/acp-20-12795-2020, 2020.

Zhao, B., Liou, K.-N., Gu, Y., Jiang, J. H., Li, Q., Fu, R., Huang, L., Liu, X., Shi, X., Su, H., and He, C.: Impact of aerosols on ice crystal size, Atmos. Chem. Phys., 18, 1065-1078, https://doi.org/10.5194/acp-18-1065-2018, 2018.

Zhou, C., Zhang, X., Gong, S., Wang, Y., Xue, M.: Improving aerosol interaction with clouds and precipitation in a regional chemical weather modeling system, Atmos. Chem. Phys., 16, 145-160, 2016.